LUIP 9202

ON INTERMITTENCY IN HEAVY ION COLLISIONS AND THE IMPORTANCE OF γ-CONVERSION IN A MULTI-DIMENSIONAL INTERMITTENCY ANALYSIS

(EMU01-collaboration)

M I Adamovich[13], M M Aggarwal[4], Y A Alexandrov[13], N P Andreeva[1], Z V Anzon[1], R Arora[4], F A Avetyan[19], S K Badyal[8], E Basova[16], K B Bhalla[7], A Bhasin[8], V S Bhatia[4], V G Bogdanov[9], V I Bubnov[1], T H Burnett[15], X Cai[18], I Y Chasnikov[1], L P Chernova[17], M M Chernyavsky[13], G Z Eligbaeva[1], L E Eremenko[1], A S Gaitinov[1], E R Ganssauge[12], S Garpman[11], S G Gerassimov[13], J Grote[15], K G Gulamov[17], S K Gupta[7], H H Heckman[3], H Huang[18], B Jakobsson[11], B Judek[14], S Kachroo[8], F G Kadyrov[17], G S Kalyachkina[1], E K Kanygina[1], M Karabova[6], G L Kaul[8], S P Kharlamov[13], T Koss[15], S A Krasnov[6], V Kumar[7], P Lal[7], V G Larionova[13], V N Lepetan[1], L S Liu[18], S Lokanathan[7], J Lord[15], N S Lukicheva[17], S B Luo[10], L K Mangotra[8], N A Marutyan[19], N V Maslennikova[13], I S Mittra[4], S Mookerjee[7], H Nasrulaeva[16], S H Nasyrov[16], V S Navotny[17], G I Orlova[13], I Otterlund[11], H S Palsania[7], N G Peresadko[13], N V Petrov[16], V A Plyushchev[9], W Y Qian[18], R Raniwala[7], S Raniwala[7], N K Rao[8], V M Rappoport[13], J Ravina[17], J T Rhee[12], N Saidkhanov[17], N A Salmanova[13], L G Sarkisova[19], V R Sarkisyan[19], G S Shabratova[6], T I Shakhova[1], D Skelding[15], K Söderström[11], Z I Solovjeva[9], E Stenlund[11], S C Strausz[15], J F Sun[5], L N Svechnikova[17], K D Tolstov[6], M I Tretyakova[13], T P Trofimova[16], U Tuleeva[16], S Vokal[6], H Q Wang[18], Z Q Weng[5], R J Wilkes[15], G F Xu[2], D H Zhang[10], P Y Zheng[2], S I Zhokhova[17] and D C Zhou[18]

1) Alma Ata, Inst. of High Energy Physics, CIS
2) Beijing, Academica Sinica, People's Republic of China
3) Berkeley, Lawrence Berkeley Lab, USA
4) Chandigarh, Panjab University, India
5) Changsa, Hunan Education Institute, People's Republic of China
6) Dubna, JINR, CIS
7) Jaipur, University of Rajasthan, India
8) Jammu, University of Jammu, India
9) Leningrad, V G Khlopin Radium Institute, CIS
10) Linfen, Shanxi Normal University, People's Republic of China
11) Lund, University of Lund, Sweden
12) Marburg, Philipps University, BRD
13) Moscow, Lebedev Institute, CIS
14) Ottawa, NRC, Canada
15) Seattle, University of Washington, USA
16) Tashkent, Institute of Nuclear Physics, CIS
17) Tashkent, Physical-Technical Institute, CIS
18) Wuhan, Hua-Zhong Normal University, People's Republic of China
19) Yerevan, Physical Institute, CIS

ABSTRACT

Non-statistical fluctuations are used to probe the dynamical behaviour of multiparticle production in heavy ion interactions at ultra-relativistic energies. In a one-dimensional analysis a $1/\langle\rho\rangle$-scaling is established and it is

furthermore found that effects from higher order particle correlations are small. In a two-dimensional analysis it is shown that a small background of particle-pairs with a narrow opening angle can distort the observed signal. As an example we estimate of the influence of γ-conversion and find that in our experiment γ-conversion alone gives results consistent with the experimental observations from a two-dimensional analysis. Whereas a two-dimensional analysis filters events where two particles are extreemely close in phase space, the one-dimensional analysis picks out events with particles clustered in pseudorapidity, which are at the same time diluted in the azimuthal plane.

1. INTRODUCTION

The topic of non-statistical fluctuations in the particle densities has attracted a lot of interest during recent years. Great efforts have been devoted to the understanding of these phenomena, but more theoretical work is still needed for the full understanding of these effects. In e^+e^--anihilation experiments the effects are at least qualitatively understood, but in hadron-hadron interactions and particularly in heavy ion interactions the effect is far from a satisfactory explanation. Experimental results and theoretical endeavours are summarized in refs [1-3].

The EMU01-collaboration has utilized two different emulsion techniques; ordinary emulsion stacks, exposed parallel to the emulsion plates, and emulsion chambers, irradiated perpendicular to the plates. Some of the chambers are equipped with thin target foils of gold, so that studies with a heavy target are feasible. The measurements in the chambers are performed with semi-automatic measurement devices[4], whereas the stacks are measured with standard techniques[5,6]. With the chamber technique a resolution of 0.013 units of pseudorapidity is obtained in the central region and a corresponding number for the stack data is better than 0.1 units. Data has been collected using the oxygen- and sulfur-beems at the CERN/SPS and the oxygen- and silicon-beams at the BNL/AGS. The data is summarized in Table 1, where also the present statistics is given. The centrality criterion used by the collaboration is based on the number of charges, Q_{z_D}, left in the spectator part of the projectile nucleus. These charges are to be found within a narrow forward cone, outside of which essentially all pareticipant matter is scattered and all produced particles are emitted. A large value of Q_{z_D} thus corresponds to a peripheral event, whereas a small value indicates a rather central or violent interaction[5].

Apart from the heavy-ion data, the collaboration has access to proton induced

interactions at comparable energies, providing a suitable environment for studies of the energy and mass dependence of different aspects of the particle production in nuclear interactions. It is quite uniqe for one experiment to have access to such a variety of data taken with essentially the same conditions.

2. FLUCTUATIONS IN ONE DIMENSION

2.1 Stochastic Emission

Due to the nuclear geometry one expects that the produced particles in heavy-ion collisions come from a large number of sources[7]. One can thus expect that most of the correlations between the produced particles will be washed out. Let us consider a pseudorapidity intervall $\Delta\eta$, within which we look at the smaller window $\delta\eta$. If we assume that correlations between particles can be neglected and that the shape of the pseudorapidity distribution is independent of the multiplicity (or centrality), we obtain that $F_2(\eta,\delta\eta) \equiv \langle n\cdot(n-1)\rangle/\langle n\rangle^2$ is independent of the size and location of the window. F_2 is generally larger than unity due to the width of the global multiplicity distribution. Whenever $\langle n\rangle\cdot(F_2-1)^{\frac{1}{2}}$ is large enough we find[8,9]

$$\sigma_2 \simeq \langle n\rangle\cdot\sqrt{F_2-1} + \frac{1}{2\cdot\sqrt{F_2-1}} \qquad (1)$$

i e we have a linear relationship between σ_2 and $\langle n\rangle$ for different windows, $\delta\eta$. Both the slope and the intercept are determined by F_2. Similar expressions are obtained for higher moments. For instance, it is found that $\sigma_3 \equiv \langle(n-\langle n\rangle)^3\rangle^{1/3}$ depends linearly on $\langle n\rangle$, where now both the slope and the intercept are given by F_2 and F_3.

Fig 1 shows some examples where these ideas are tested for the second and third orders, for η-windows centered around midrapidity. We find a nice linear behaviour as long as the windows are narrow enuogh to exclude the fragmentation regions. These results clearly indicate that this kind of stochastic emission works well in the central region and that the correlation between the produced particles are well hidden in the combinatorial background. Thus the intermittency effect is, in a global sence, only a tiny effect, and is normally not seen, unless special tools are utilized in the analysis.

We shall return to these ideas in section 2.3. where the error estimates of

and the intercorrelations between scaled factorial moments are discussed.

2.2 Scaled Factorial Moments

The most commonly used methods for studying non-statistical fluctuations are introduced in two papers by Białas and Pechanski[10]. These methods are based on the notion of scaled factorial moments and differ in the procedures of normalization and how to average over events and over different regions of phase space. One method, horizontal averaging, calculates the moments for each event and then averages over the events. A second method, vertical averaging, first calculates the moments for a given η-bin in all events and then averages over all bins. Horizontal averaging is normally followed by a correction for the variation of particle densities as a function of η, normally referred to as Fialkowski correction[11]. The moments can either be normalized to the whole event sample or to the individual events (individual bins for the vertical averaging). The moments are studied as a function of the chosen η-bin and the variation of the moments with varying $\delta\eta$ may indicate an intermittent behaviour.

The very good resolution of our chambers allows us to study a region which is normally not accessible for other fixed target experiments. In fig 2 we show results for central ^{32}S+Au events[12] calculated with the vertical method, i e

$$\langle F_q \rangle_V = \frac{1}{M} \cdot \sum_{m=1}^{M} \frac{1}{N_{ev}} \cdot \sum_{i=1}^{N_{ev}} \frac{k_{m,i} \cdot (k_{m,i}-1) \cdot \cdots \cdot (k_{m,i}-q+1)}{\langle k_m \rangle^q} \tag{2}$$

where

$$\langle k_m \rangle = \frac{1}{N_{ev}} \cdot \sum_{i=1}^{N_{ev}} k_{m,i} \tag{3}$$

Here N_{ev} is the number of events in the sample, $k_{m,i}$ is the content of bin m in event i, and M is the number of bins. Also indicated in the figure are the results obtained by horizontal averaging, i e

$$\langle F_q \rangle_H = \frac{1}{N_{ev}} \cdot \sum_{i=1}^{N_{ev}} M^{q-1} \cdot \sum_{m=1}^{M} \frac{k_{m,i} \cdot (k_{m,i}-1) \cdot \cdots \cdot (k_{m,i}-q+1)}{\langle N \rangle^q} \tag{4}$$

where $\langle N \rangle$ is the average multiplicity in the full η-region. The horizontal results are furthermore shape-corrected by dividing by the Fialkowski-factor[11]

$$R_F(q,M) = \frac{1}{M} \cdot \sum_{i=1}^{M} M^q \frac{\langle k_m \rangle^q}{\langle N \rangle^q} \qquad (5)$$

As can be seen in the figure, the two methods give essentially the same results. The FRITIOF model[13] shows no variation with $\delta\eta$ (not shown in the figure). We conclude that for $\delta\eta > \sim 0.1$ the moments rise with decreasing $\delta\eta$, but for smaller values of $\delta\eta$ the moments show a weaker dependence on $\delta\eta$. The rise of the moments for $\delta\eta > \sim 0.1$ is consistent with other experimental findings[14].

In fig 3 we show $\ln(F_q)$, calculated with the horizontal method, versus $-\ln(\delta\eta)$ for a central sample of ^{16}O+Em interactions at 200 A GeV before and after the shape correction. Here the full η-window is restricted to the central region, $|\eta - \eta_{cm}| < 1$, and the $\delta\eta$-region is chosen to be 0.1 - 2. As can be seen in the plot, the correction is marginal at this energy and furthermore that within the studied region the linearity is quite good.

2.3 Slopes of Scaled Factorial Moments

When straight lines are fitted to data as in fig 3, a few facts have to be kept in mind. For a given moment the points are strongly correlated since the same sample is used, although with a different binning, for each point. This makes it very hard to estimate the error of the intermittency index, ϕ_q, i e the slope of the line. Furthermore for the same reason the different moments are strongly correlated, which will be discussed further in section 2.4. In order to estimate the errors of the slopes we have devised a simple Monte Carlo method based on the stochastic emission picture in section 2.1. As input we use the experimentally observed multiplicity and pseudorapidity distributions and particles are randomly emitted. The MC-samples are generated exactly as large as the corresponding experimental samples. For every one of the experimental samples N_{MC} similar MC-samples are generated, and from

$$\sigma(\phi) \simeq \sqrt{\langle \phi^2 \rangle - \langle \phi \rangle^2} \qquad (6)$$

the standard deviation of the slope, ϕ_q, is estimated. This estimate has an uncertainty of $(2 \cdot N_{MC})^{-\frac{1}{2}}$ and to reach an acceptable level, e q 7 %, we need $N_{MC} = 100$. Due to the non-statistical fluctuations, however small, this procedure may underestimate the errors somewhat and this effect is expected to grow with increasing moments.

Eq (4) can be seen as a sum multiplied by a normalization factor. Since high multiplicity events have a larger propability for large local particle densities they will provide the largest contributions to the sum. These events will thus influence the intermittency-indices more than events with lower multiplicities in cases where samples of events from a broad distribution are studied. This is even more so for higher order moments. This effect was investigated in our combined (biased towards high multiplicities) ^{16}O+Em sample at 200 A GeV. Out of a total of 791 events a multiplicity cut, $n > n_{cut}$, was applied, and fig 4 shows the results of ϕ_3 and ϕ_6 as a function of n_{cut}. For small values of n_{cut} it is clearly seen that the slopes and the error estimates are essentially independent of n_{cut}, whereas the intercepts decrease due to the change in the normalization factor. A noticeable change in slopes (and errors) is only seen when less than 20 % of the events remain. We thus come to the conclusion that in heavy-ion experiments, where the multiplicities are varying in a wide range, nothing is gained by treating full samples. Information is normally gained if subsamples with a limited multiplicity range are studied.

2.4 Scaling Rules

Several scaling rules for factorial moments and intermittency.indices have been proposed in the literature. Seibert[15] and others have proposed a relationship between F_q and the average particle density based on the assumption that only two-particle correlations are present. For instance, $F_2 - 1$ reflects the ratio between the number of real correlated pairs and the number of combinatorial pairs and would thus be inversely proportional to the particle density. Since for $F_2 \simeq 1$ we have $\ln(F_2) \simeq F_2 - 1$, the same would be expected for ϕ_2. This scaling rule is tested in fig 5, where ϕ_2 is plotted versus $\langle\rho\rangle$ for different central and semi-central samples[16]. Except for the sulfur-induced interactions all samples are well described by the same $\langle\rho\rangle^{-1}$-curve independent of energy and centrality cut. The sulfur-induced samples seem to violate the trend and show larger slopes than expected. When the $\langle\rho\rangle^{-1}$-curve is extrapolated down to the region of hadron-induced interactions[17] it seem to reproduce the intermittency-indices observed for this kind of interactions. All these data samples have been analyzed in exactly the same way ($|\eta-\eta_{cm}| < 1$ and $0.1 < \delta\eta < 2.$), which is necessary in order to obtain an unbiased plot.

Another scaling rule which relates indices of different orders is given by[10]

$$\phi_q = \binom{q}{2} \cdot \phi_2 \tag{7}$$

which again is valid in the case of pure two-particle correlations. Multi-particle correlation functions contain components from correlation functions of lower orders. Factorial moments, being integrals of correlation functions, will have the same shortcoming, and so will the intermittency-indices. If now also true three-particle correlations are considered, eq (7) can be changed to include those.

$$\phi_q^{(3)} = \binom{q}{3} \cdot \phi_3 - (q - 3) \binom{q}{2} \cdot \phi_2 \tag{8}$$

which reduces to eq (7) for $\phi_3 = 3 \cdot \phi_2$, can be seen as the next expression in a series of expressions taking increasing orders of correlations into account. The bracketed index indicates the highest order of correlations considered. With the normalized slopes defined as

$$\zeta_q \equiv \phi_q \; / \binom{q}{2} \tag{9}$$

we can reformulate eq (8) as

$$\zeta_q^{(3)} = (q - 2) \cdot \zeta_3 - (q - 3) \cdot \zeta_2 \tag{10}$$

i e we get a linear relationship between ζ_q and q. Eq (10) has been tested in fig 6 for different central heavy ion samples, and indeed all the tested samples are in good agreement with eq (10). This indicates that it is sufficient to consider only correlations of the second and third orders, or in other words the values of ζ_q for $q \geq 4$ can be well understood from the values of ζ_2 and ζ_3. However, when the differences $\zeta_3 - \zeta_2$ are studied for the different data samples and compared to the same differences in MC-samples, created as in section 2.3, we find, within the statistical uncertainties, that these differences are essentially consistent with being zero. We can thus, with the present statistics, not exclude the scaling rule given by eq (7). With the same arguments which led to the $\langle\rho\rangle^{-1}$-scaling above we see that higher order contributions will scale as $\langle\rho\rangle^{-\alpha}$, with $\alpha > 1$, showing that it will be increasingly hard to detect higher order contributions in a high multiplicity environment.

The anomalous fractal dimensions, d_q, related to ϕ_q by

$$d_q = \frac{\phi_q}{q - 1} \tag{11}$$

are claimed to be sensitive to the nature of phase transitions[18]. A d_q which is independent of q could be taken as an indication of a second-order phase transition. If eq (7) is true, a second-order phase transition would be ruled out, and, as we discussed above, the data is consistent with eq (7).

2.5 Influences from γ-Conversion

Electron-pairs produced either by direct Dalitz-decay or through γ-conversion may be partly responsible for the observed intermittency effects. FRITIOF-simulations, where γ-conversion is added[19], have been used to study the influence of those processes on the intermittency-indices. The results from the simulations are found to follow the same scaling rules as discussed in the previous section. With p being the percentage of the gammas which give rise to electrons which are measured along with the produced hadrons, our findings can be parametrized as

$$\phi_{q,\mathrm{pair}} \simeq \kappa \cdot \binom{q}{2} \cdot \frac{p}{\langle\rho\rangle} \tag{12}$$

where κ is an experimental parameter which depends on the choice of $\Delta\eta$-window and $\delta\eta$-range. The influence of Dalitz-production on the intermittency-indices is found to be negligable. For all data samples in fig 5, where $\kappa = 0.033$, the percentage, p, is such that the influence on the indices from γ-conversion is smaller than or compatibel with the quoted statistical errors.

2.6 The η-Dependence of the Intermittency-Indices

Figure 7 shows the influence of window location on the extracted ϕ_2 values. The results suggest that also the η-dependence can be described by $1/\langle\rho\rangle$-scaling, although better statistics is needed for further investigations. The curve is obtained as the inverse of the average pseudorapidity distribution. The parameter 0.315 is obtained from fig 5 for the sulfur-induced interactions; no further parameters are introduced. Particles with $\eta \leq 1.3$ are not measured with the chamber technique. This result indicates that once the particle density is taken into account the intermittency signal is about the same in different regions of phase space.

2.7 Limiting Fragmentation

It has been pointed out that pseudorapidity distributions from the same colliding system at different incident energies coincides in the target and the projectile fragmentation regions[6], which indicates that limiting fragmentation is valid in heavy-ion collisions. Results from a further investigation is shown in fig 8 where intermittency-indices for the second and third orders are plotted for central ^{16}O+Em interactions at 60 and 200 A GeV[20]. In order to cope with the rapidly changing particle densities in the said regions the pseudorapidity variable, η, is transformed into the variable χ defined as[21]

$$\chi(\eta) = \frac{\int_{\eta_1}^{\eta} \rho(\eta')\, d\eta'}{\int_{\eta_1}^{\eta_2} \rho(\eta')\, d\eta'} \tag{13}$$

so that χ is uniformly distributed in the interval 0 to 1. As can be seen in the figure the results from the two energies are similar, supporting the idea of limiting fragmentation.

2.8 Alternative Approaches

One alternative method of isolating effects from a given order is by means of factorial cumulants[22]. Factorial moments and factorial cumulants are related and the few first orders are given by

$$K_2 = F_2 - 1 \tag{14}$$

$$K_3 = F_3 - 3\cdot(F_2 - 1) - 1 \tag{15}$$

and as the order increases the expressions grow more complex. In fig 9 we show scaled factorial cumulants for central ^{32}S + Au interactions at 200 A GeV calculated with vertical averaging. As can be seen in the figure already the third order cumulants are essentially zero which supports the findings discussed in section 2.4.

Also worth attention are the factorial correlators[23]. Such correlators do not only measure the amount of non-statistical fluctuations, but also correlates

these fluctuations in different regions of phase space. In fig 10 some results for ^{32}S + Em interactions at 200 A GeV are shown. Here the logarithm of the factorial correlators $\langle F_{pq} \rangle$ defined as

$$\langle F_{pq} \rangle = \frac{1}{M^*} \cdot \sum_{m=1}^{M^*} \frac{\langle k_m \cdot (k_m-1) \cdot \cdots \cdot (k_m-p+1) \cdot k_{m'} \cdot (k_{m'}-1) \cdot \cdots \cdot (k_{m'}-q+1) \rangle}{\langle k_m \cdot (k_m-1) \cdot \cdots \cdot (k_m-p+1) \rangle \cdot \langle k_{m'} \cdot (k_{m'}-1) \cdot \cdots \cdot (k_{m'}-q+1) \rangle} \qquad (16)$$

where m and m′ are two bins with a distance D and $M^* = (\Delta\eta - D) \cdot M/\Delta\eta$ (M is the number of $\delta\eta$-bins in the $\Delta\eta$-window as before), are plotted as a function of -ln(D). In this figure $\delta\eta$ is chosen to be 0.1 rapidity units. As can be seen the correlations grow with decreasing distance D.

There are other methods proposed in the litterature but several of those might not be sensitive enough to detect the small non-statistical fluctuations present in heavy-ion collisions, and their merits have to be proven before they can be taken seriously.

2.9 Conclusions from the One Dimensional Analysis

We end this chapter by the following conclusions. In a limited $\delta\eta$-range ($0.1 < \delta\eta < 2$) the intermittency-indices, ϕ_q, are constant. For a given system ϕ_2 follows a $1/\langle\rho\rangle$-dependence, but normalized to the same density, the largest systems show somewhat larger slopes. The data seems to be consistent with the scaling rule given by eq (7). Thus ϕ_q versus $\langle\rho\rangle$ will look similar to ϕ_2 versus $\langle\rho\rangle$ but with increased experimental errors. We also conclude that essentially all statistically significant information can be extracted from second order moments. To go beyond the information contained in two different orders requires a substantial increase in statistics. The systematic errors introduced by electron-pairs influences the data, but can only partially explain the observed slopes. This is however not the case when the analysis is performed in two-dimensions as we will see in the next chapter.

3. FLUCTUATIONS IN TWO DIMENSIONS

3.1. Scaled Factorial Moments in Two Dimensions

The definition of the scaled factorial moments in a two dimensional space is quite straight forward; the only change in eqs (2) and (4) is that now M is the number of $\delta\eta\delta\varphi$-bins, where φ is the azimuthal angle of an emitted particle.

A typical result from the two-dimensional procedure is shown in fig 11 a), in this case $\langle F_2 \rangle_H$ for central ^{32}S + Au interactions at 200 A GeV. The $\delta\eta$-axis ranges from 2 down to 0.016 ($|\eta - \eta_{cm}| < 1$) and the $\delta\varphi$-axis ranges from $2 \cdot \pi$ to $0.016 \cdot \pi$; in both directions one step corresponds to a factor of two more bins. Thus the innermost channel corresponds to ~16000 bins. Fig 11 b) shows the same data Fialkowski-corrected along the η-direction but, as in the one-dimensional case, this correction is small. F_q for higher orders looks essentially the same (fig 12), but with our limited statistics the uncertainties become large.

In order to study back-to-back correlations one can redefine the azimuthal bins according to fig 13 (right part) and in fig 14 the results of this azimuthal folding are shown. As it turns out the signals decrease with azimuthal folding from which we conclude that the main effects originate from particles close by in azimuth.

3.2 One-Dimensional Slices

We can now slice the two-dimensional histograms in different ways. It can be sliced along the main diagonal (fig 15, top left). This slice is the only one which has been studied in experimental investigations[24] so far. Other slices of interest are summarized in fig 15; slice along the cross-diagonal keeping the total number of bins fixed (top right) and slices perpendicular to one of the axes keeping either $\delta\varphi$ (lower left) or $\delta\eta$ (lower right) fixed.

Fig 16 a) shows the outcome for slices along the $\delta\eta$-axis of fig 11 b) keeping $\delta\varphi$ fixed. The lines are fits in the region $M = 2^2 - 2^7$, where the linearity is reasonable. For decreasing $\delta\varphi$ we find that the slope fastly increases. A similar behaviour is seen for slices in the other direction in fig 16 b).

Fig 17 shows the slice along the main diagonal, which clearly indicates a stronger than linear dependence. Such a dependence is expected from the behaviour in fig 16, as illustrated by a simple numerical example in fig 18.

Along the cross-diagonal, fig 19, we find a rather flat spectrum with a maximum for $M_\eta \simeq M_\varphi$. In fact, in a scenario with randomly oriented pairs of particles, one would expect a maximum for $\delta\eta = \delta\varphi$, corresponding to $\ln M_\varphi \simeq 3$. This indicates that what we see in our two-dimensional analysis may be attributed to some kind of pair-production, as we will see in section 3.4, to γ-conversion.

3.3 One-Dimensional Slopes in Slices along the Axes

In fig 20 the slopes obtained from the fitted lines in fig 16 are shown. As can be seen the data points essentially follows the dashed lines indicated in the figure. These lines are obtained under the assumption that each new division doubles the slope. This is exactly what occurs if each subdivision of the events results in new uncorrelated subevents. We thus have the inverse situation to that discussed in section 2.4 in connexion with the $1/\langle\rho\rangle$-rule. However, this trend is brooken when the number of subdivisions is large enough. What actually happens when the bins are smaller than the typical extension of an electron-pair from a γ-conversion, is that pairs of correlated particles are starting to end up in different bins, and the climb along the dashed line is hindered. The average opening angle of an electron-pair agrees well with the point at which the data roll off from the lines of slope = 1.

3.4 The Influence of γ-Conversion

The same MC-procedure as was used in section 2.5 is now applied to the two-dimensional analysis. For the ^{32}S + Au we estimate that 3 % of the produced gammas convert, the majority of them in the target gold-foil. Fig 21 shows the outcome of the MC-calculation analyzed in two dimensions and it is in the essentials well corresponding to fig 11 b). The FRITIOF-model itself, without γ-conversion, gives an essentially flat distribution. Furthermore, it is found that size of the fluctuations are proportional to the percentage of converted gammas (cf eq(12)).

The same steps, which led to fig 20, are now applied to the MC-data, resulting in figs 22. The comparison between the real data and the MC-data clearly shows that the intermittency effect drowns in the background from γ-conversion when the two-dimensional procedure is applied.

The whole procedure is repeated for a sample of central ^{16}O + Em interactions at 200 A GeV. Here the emulsion itself works as the target and the unresolved γ-conversion is estimated to be $\simeq$ 1 %. Also for this sample the obtained results indicate that the intermittency signal is completely hidden in the γ-conversion background. In fig 23 we show the slopes obtained along the axes for the sample of central ^{16}O + Em interactions at 200 A GeV, and as we can see the similarities with fig 20 are quite obvious.

3.5 Repeated Analysis in a Restricted Region of M

In section 3.2 the M-region used for the fitting was chosen to be 2^2 to 2^7. In order to study where the γ-conversion starts to kill the intermittency signal, we have repeated the two-dimensional analysis in the restricted region $M = 2^0$ to 2^4 (fig 24). Fig 25 shows the results for the ^{32}S + Au data. As can be seen the MC-data still follows the dashed line, but the real data has a weaker dependence. At large ln M the two sets coincide. This clearly indicates that, when only one dimension is utilized, the experimentally observed effect is larger than expected from γ-conversion. As soon as cuts are applied in both dimensions the net effect dies off. Essentially the same results are obtained for the ^{16}O + Em data.

3.6 Particle-Correlations in the FRITIOF-Model

As has been mentioned earlier (see sections 2.2 and 3.4) the FRITIOF-model seems to show no intermittency signal what-so-ever. One may thus ask whether there are any particle-correlations in such a model. The answer is yes, as illistrated in fig 26, which shows two-particle correlations measured in pp-collisions at ISR-energies[25]. The data (points) and the results from the FRITIOF-calculation (histogram) agree qualitatively, althogh minor deviations are seen, especially in the semi-inclusive case.

3.7 Conclusions from the Two-Dimensional Analysis

We end this chapter with the following conclusions. In the two-dimensional analysis the data is strongly influenced by γ-conversion. The two-dimensional procedure seems to work as a filter for the electron-pairs. This means, however, that the correlations which gives the largest contributions to the one-dimensional moments are not the same as the once which are contributing to the two-dimensional moments. It indicates that the bulk of the events responsible for the one-dimensional effect are of 'ring-type', i e strong correlations in η, diluted over the whole 2π in ϕ. A scatterplot of the event from the central ^{32}S + Au sample which gives the largest contribution to the one-dimentional F_2 is shown in fig 27, where also the two bins which gives the largest contributions are indicated. Similarly the event from the same sample which gives the largest contribution to the two-dimensional F_2 is shown in fig 28. Also here the most important bins are indicated. The two figures gives an idea of how small the intermittent effects are; it is not easy to pick out the main contributions

by the naked eye. On the other hand the eye, a superiour instrument for pattern recognition, seem to register a lot of structure in plots like figs 27 and 28.

4. SUMMARY

In this last chapter we would like to sum up our results obtained so far.

$1/\langle\rho\rangle$-scaling is observed for different interacting systems, for different incident energies and possibly also for different η-regions. The same is to some extent also true for the subevents in the sense of section 3.3.

The data is consistent, within the statistical uncertainties, with the scaling expressed by eq (7), which relates indices of different orders.

One-dimensional results in η or in φ are essentially the same (cf fig 25).

The two-dimensional analysis is saturated by γ-conversion. In other experiments where γ-conversion is important, and in experiments using electronic tracking-devices where 'ghost tracks', i e tracks that are split into two, may appear, one should not only look at a slice along the main diagonal, but rather use the full multi-dimensional distribution to get a handle on the different background-producing sources.

The total observed effect may very well be the sum of different physical phenomina. Here effects from string fragmentation and hadronic decays, HBT (should influence the region $\delta\eta \sim 0.1 - 0.5$ depending on the radius), and γ-conversion may be of importance.

ACKNOWLEDGEMENTS

The financial support from the Swedish Natural Science Research Council, the German Federal Minister of Research and Technology, The University Grants Commission, Gouvernment of India, The National Science Foundation of China, The Distinguished Teacher Foundation of the State Education Commission of China, The Fok Ying Tung Education and The US Department of Energy and National Science Foundation are gratefully acknowledged.

REFERENCES

[1] Proc Santa Fe Workshop on Intermittency in High Energy Collisions, Los Alamos National Laboratory, Los Alamos, USA, March 18-21, 1990 (Eds: F Cooper, R C Hwa, I Sarcevic, World Scientific), and references therein.

[2] Proc Int Workshop on Correlations and Multiparticle Production (CAMP - LESIP IV), Marburg, F R Germany, May 14 - 16, 1990 (Eds: M Plümer, S Raha, R M Weiner, World Scientific), and references therein.

[3] Proc Ringberg Workshop on Multiparticle Production, Fluctuations and Fractal Structure, Ringberg Castle, Germany, June 25-28, 1991 (to appear as a World Scientific publication), and references therein.

[4] S Garpman et al, Nucl Instr & Meth **A269**(1988)134.

[5] M I Adamovich et al (EMU01-collaboration), Phys Lett **B223**(1989)262.

[6] M I Adamovich et al (EMU01-collaboration), Rev Lett **62**(1989)2801.

[7] E Stenlund, Mod Phys Lett **A5**(1990)1159.

[8] M I Adamovich et al (EMU01-collaboration), Phys Lett **B242**(1990)512.

[9] M I Adamovich et al (EMU01-collaboration), Mod Phys Lett **A6**(1991)469.

[10] A Białas and R Pechanski, Nucl Phys B273(1986)703; **B308**(1988)857.

[11] K Fialkowski et al, Acta Physica Polonica **B20**(1989)639.

[12] M I Adamovich et al (EMU01-collaboration), Phys Rev Lett **65**(1990)412.

[13] B Nilsson-Almquist and E Stenlund, Comp Phys Comm **43**(1987)387.

[14] See, for instance, R Holinski et al, Phys Rev Lett **62**(1989)733.

[15] D Seibert, Phys Rev **D41**(1990)3381.

[16] M I Adamovich et al (EMU01-collaboration), Phys Lett **B263**(1991)539.

[17] J Babecki et al, Acta Physica Polonica **B5**(1974)315, and private communication; I Otterlund et al, Nucl Phys **B142**(1978)445; A Abduzhamilov et al, Phys Rev **D39**(1989)86.

[18] A Białas and R Hwa, CERN preprint CERN-TH.5754/90(1990).

[19] A Borselino, Phys Rev **89**(1953)1023.

[20] M I Adamovich et al (EMU01-collaboration), "A Systematic Investigation of the Energy Independent Behaviour in the Fragmentation Regions for ^{16}O+Em Interactions from 3.7 to 200 A GeV", submitted to Z Phys C.

[21] A Białas and M Gazdzicki, Phys Lett **B252**(1990)483; W Ochs, Phys Lett **B247**(1990)101.

[22] P Carruthers, H Eggers and I Sarcevic, Phys Lett **B254**(1991)258.

[23] V V Aivazyan et al (NA22-collaboration), Phys Lett **B258**(1991)487.

[24] See, for instance, R Holinski et al, Phys Rev **C40**(1990)R2449.

[25] W Bell et al, Z Phys C22(1984)109.

Table 1: The experimental data.

		Minimum Bias[a]	Central[b]
^{16}O + Em	14.6 A GeV	697	-
^{16}O + Em	60 A GeV	690	-
^{16}O + Em	200 A GeV	534	257
^{28}Si + Em	14.6 A Gev	972	-
^{32}S + Em	200 A GeV	1103	102
^{32}S + Au	200 A GeV	-	360

[a] Events obtained from emulsion stacks.

[b] Events obtained from emulsion chambers.

FIGURE CAPTIONS

Figure 1: σ versus $\langle n_s \rangle$ for different rapidity windows for oxygen-induced interactions at different energies. The errors in each data point are in the region 4 - 6 % in both directions. The dashed lines indicate the asymptotic behaviour.

Figure 2: Scaled factorial moments calculated with two different methods.

Figure 3: Scaled factorial moments for central ^{16}O + Em interactions at 200 A GeV. Left uncorrected and right Fialkowski corrected.

Figure 4: Intermittency-indices, ϕ_q, for q = 3 and 6, as a function of the lower multiplicity cut, n_{cut}. The numbers in brackets give the number of remaining events after the cut.

Figure 5: Intermittency-indices of the second order as a function of average particle density for different systems, incident energies and centrality cuts.

Figure 6: Normalized slopes, ζ_q, as a function of the order q for different central samples. Linear fits are indicated by the lines.

Figure 7: Intermittency-indices of the second order as a function of pseudorapidity.

Figure 8: Intermittency-indices of the second and third orders for central ^{16}O + Em interactions at two different incident energies.

Figure 9: Second and third order factorial cumulants for central ^{32}S + Au interactions.

Figure 10: Factorial correlators versus the inverse gap distance. For each new correlator one unit is added to the values.

Figure 11: Scaled factorial moment, F_2, in two dimensions (logarithmic scale). a) Uncorrected. b) Corrected.

Figure 12: As fig 11 a), but for F_3.

Figure 13: Two definitions of a $\delta\varphi$-bin.

Figure 14: As fig 11 b), but with a $\delta\varphi$-bin defined as in the right part of fig 13.

Figure 15: Different slices of interest in the two-dimensional histogram.

Figure 16: Slices along the axes of fig 11 b). a) $\delta\eta$-axis. b) $\delta\varphi$-axis.

Figure 17: Slice along the main diagonal of fig 12.

Figure 18: A simple numerical example of the non-linear dependence along the main diagonal.

Figure 19: Slice along the cross-diagonal of fig 12.

Figure 20: Slopes obtained from fig 16, as a function of the number of bins used in in the other dimension. a) In the η-direction. b) In the ϕ-direction.

Figure 21: Scaled factorial moment, F_2, in two dimensions for a FRITIOF-sample with 3 % γ-conversion added (logarithmic scale).

Figure 22: As fig 20, but for the MC-generated sample from fig 21.

Figure 23: As fig 20, but for a sample of central ^{16}O + Em interactions at 200 A GeV.

Figure 24: The restricted M-region for the repeated analysis.

Figure 25: Comparison between slopes from real data and from the MC-generated sample in the restricted M-region. a) In the η-direction. b) In the ϕ-direction.

Figure 26: Demonstration of two-particle correlations in FRITIOF (histogram). Data (points) from ISR[30]. a) Inclusive. b) Semi-inclusive.

Figure 27: Scatterplot of the event which gives the main contributions in the one-dimensional analysis.

Figure 28: Scatterplot of the event which gives the main contributions in the two-dimensional analysis.

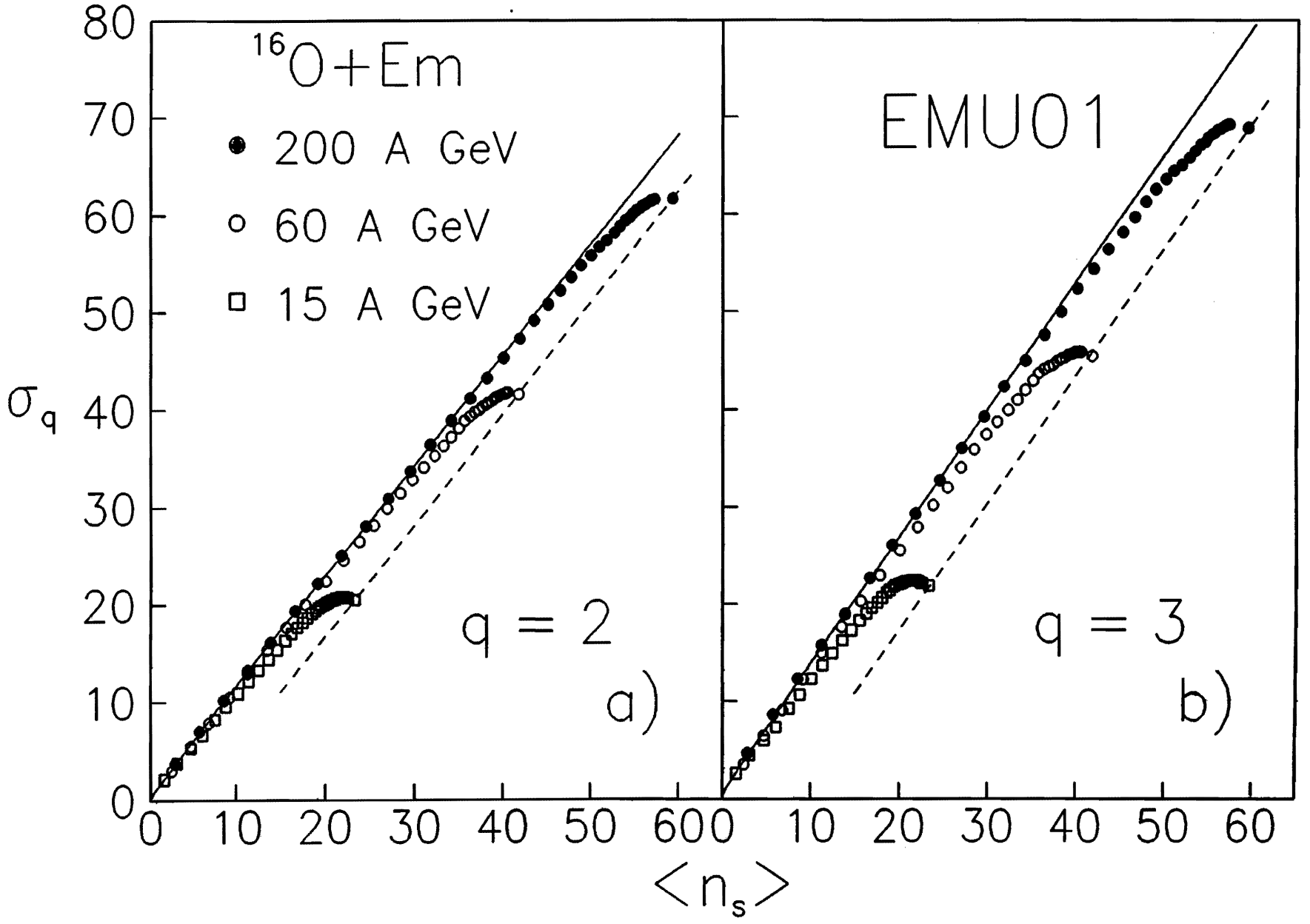
$^{16}O+Em$
200 A GeV
60 A GeV
15 A GeV
EMU01
σ_q
$\langle n_s \rangle$
q = 2
q = 3
a)
b)
0
10
20
30
40
50
60
70
80

Fig. 1

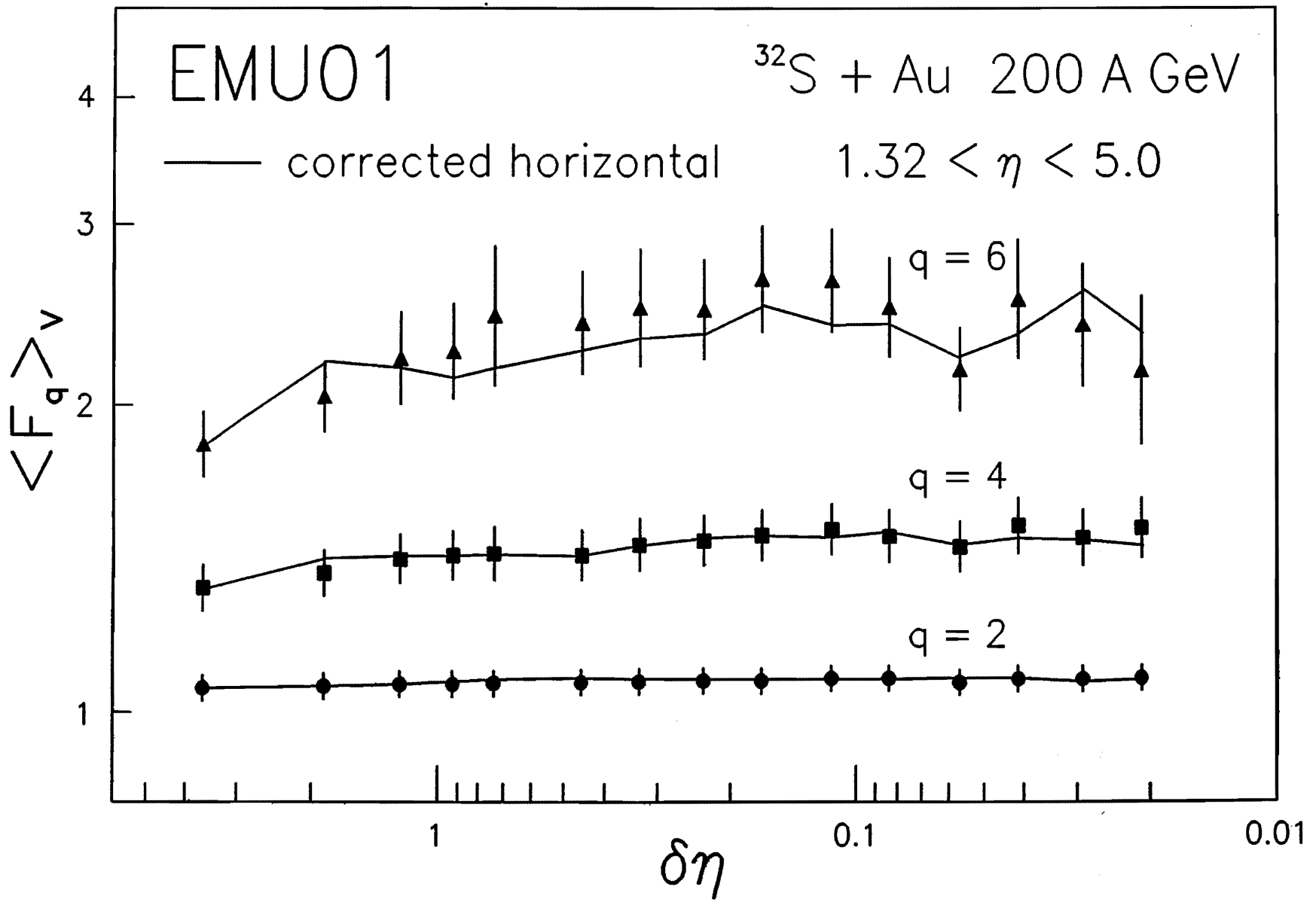
EMU01
^{32}S + Au 200 A GeV
corrected horizontal
1.32 < η < 5.0
q = 6
q = 4
q = 2
$\langle F_q \rangle_v$
4
3
2
1
1
0.1
0.01
δη

Fig. 2

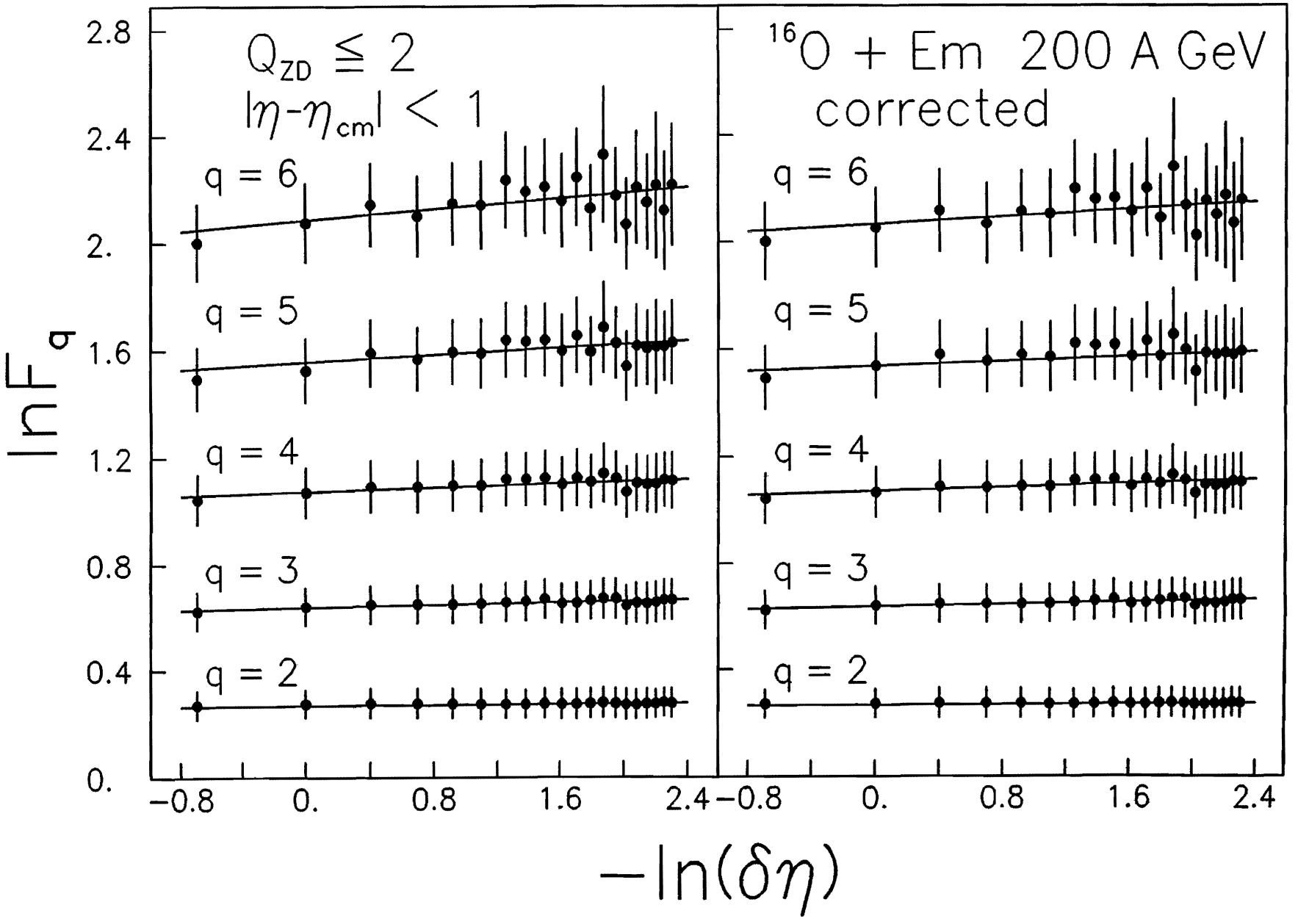
$Q_{ZD} \leqq 2$
$|\eta - \eta_{cm}| < 1$
^{16}O + Em 200 A GeV
corrected
q = 6
q = 5
q = 4
q = 3
q = 2
$\ln F_q$
$-\ln(\delta\eta)$
2.8
2.4
2.
1.6
1.2
0.8
0.4
0.
−0.8
0.
0.8
1.6
2.4

Fig. 3

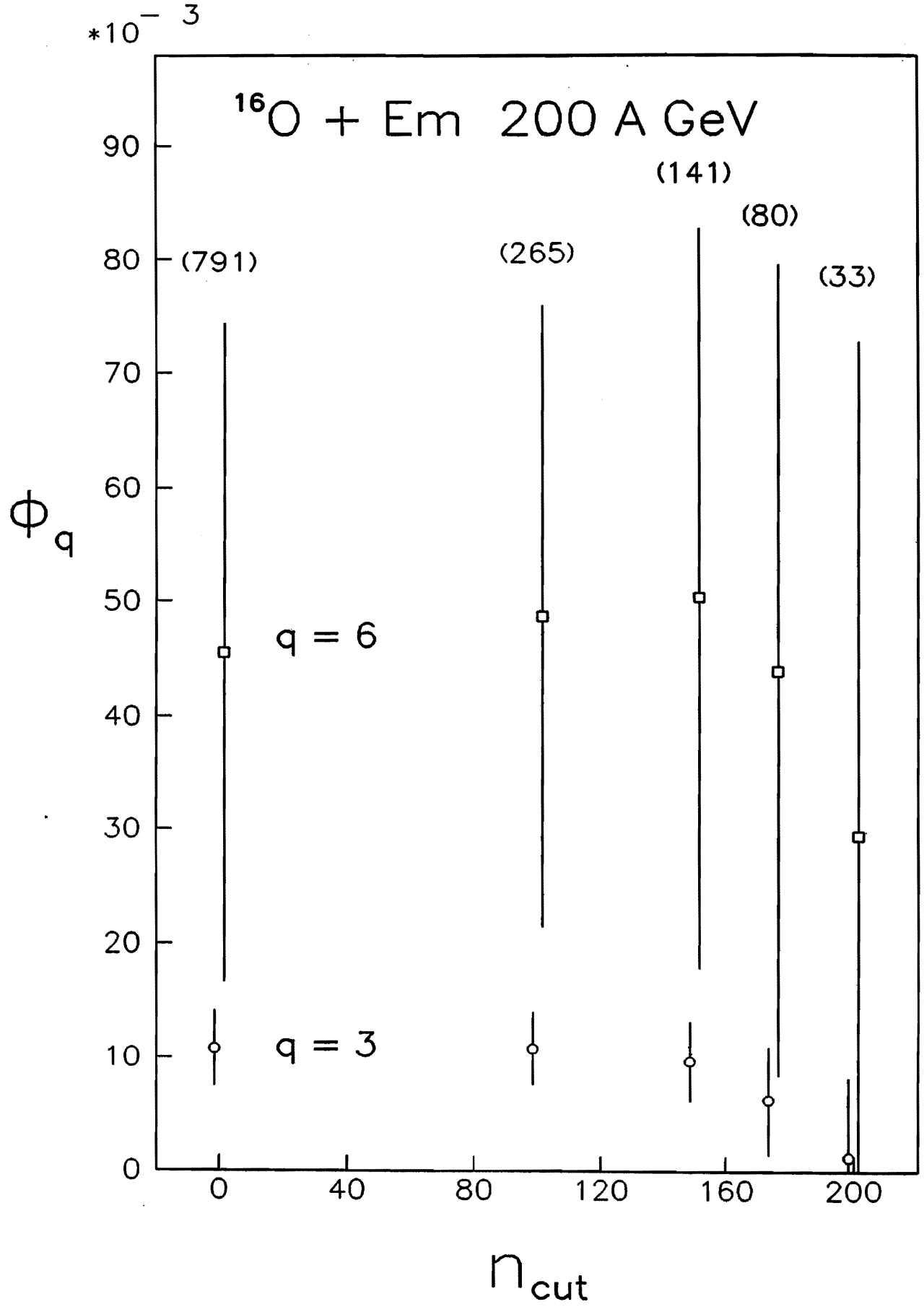
*10^-3
16O + Em 200 A GeV
(791)
(265)
(141)
(80)
(33)
q = 6
q = 3
Φq
ncut
0
10
20
30
40
50
60
70
80
90
0
40
80
120
160
200

Fig. 4

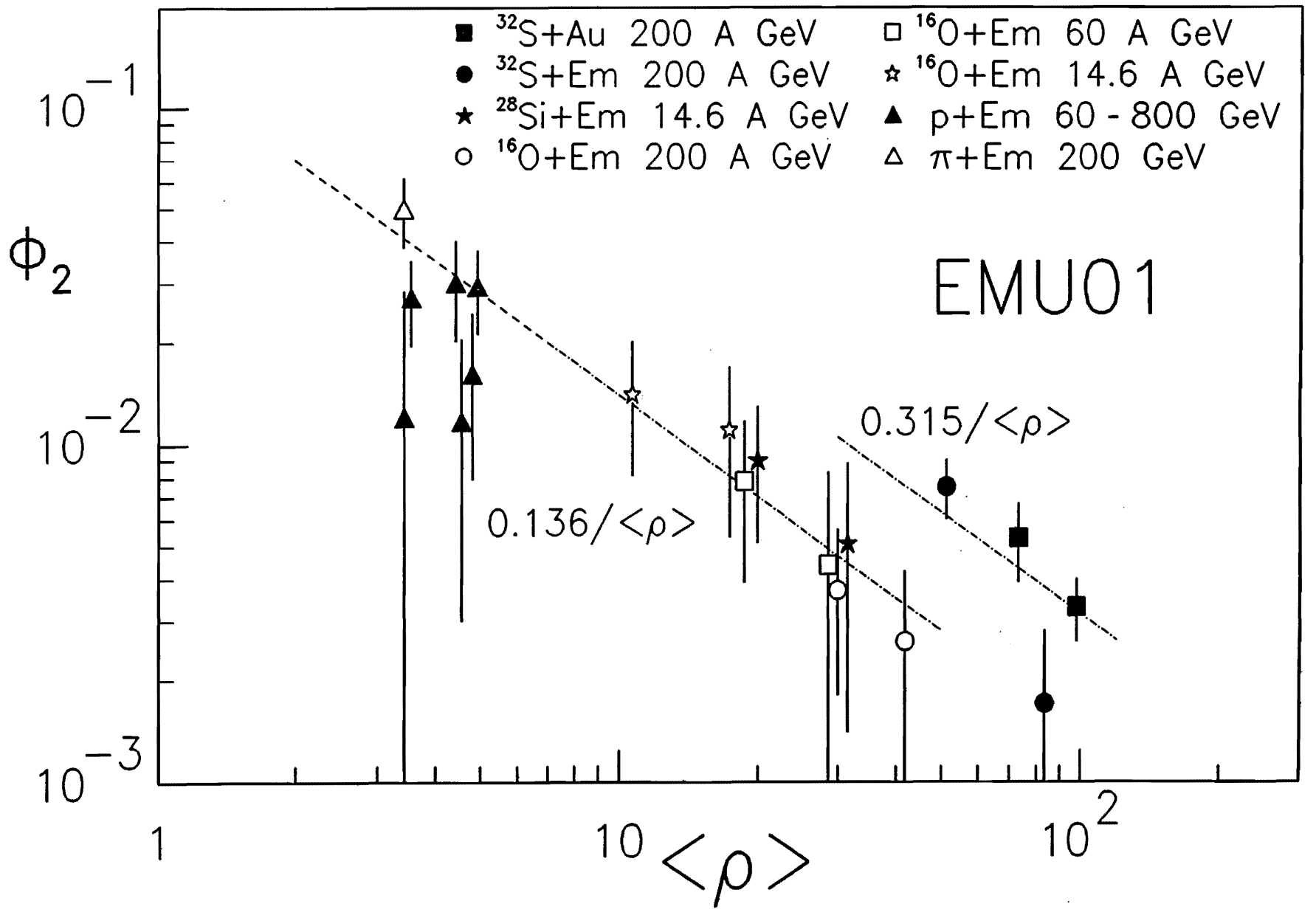
■ ^{32}S+Au 200 A GeV
● ^{32}S+Em 200 A GeV
★ ^{28}Si+Em 14.6 A GeV
○ ^{16}O+Em 200 A GeV
□ ^{16}O+Em 60 A GeV
☆ ^{16}O+Em 14.6 A GeV
▲ p+Em 60 - 800 GeV
△ π+Em 200 GeV
EMU01
Φ_2
10^{-1}
10^{-2}
10^{-3}
0.315/<ρ>
0.136/<ρ>
1
10
10^2
<ρ>

Fig. 5

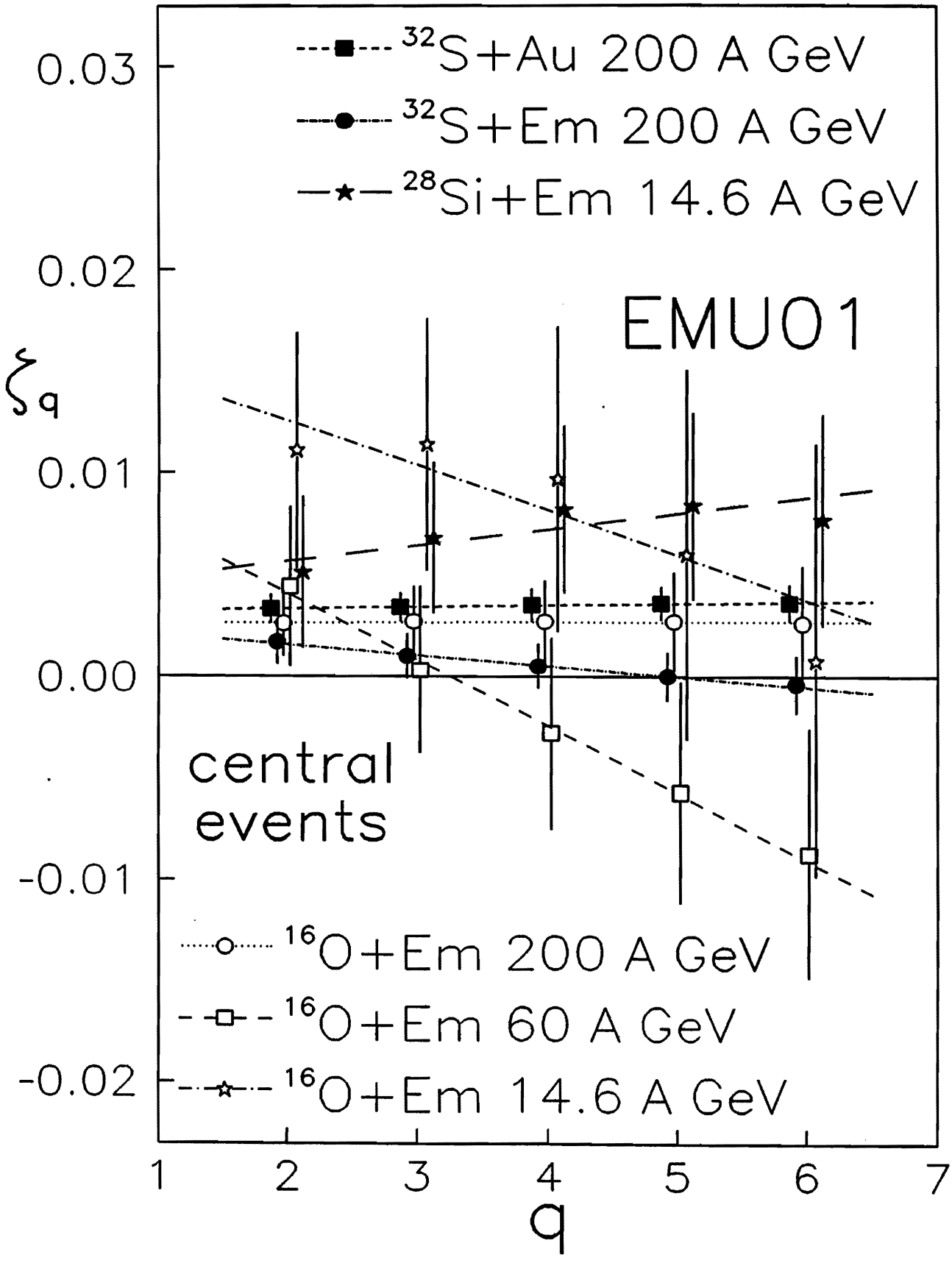
^{32}S+Au 200 A GeV
^{32}S+Em 200 A GeV
^{28}Si+Em 14.6 A GeV
EMU01
central events
^{16}O+Em 200 A GeV
^{16}O+Em 60 A GeV
^{16}O+Em 14.6 A GeV
ζ_q
q
0.03
0.02
0.01
0.00
-0.01
-0.02
1
2
3
4
5
6
7

Fig. 6

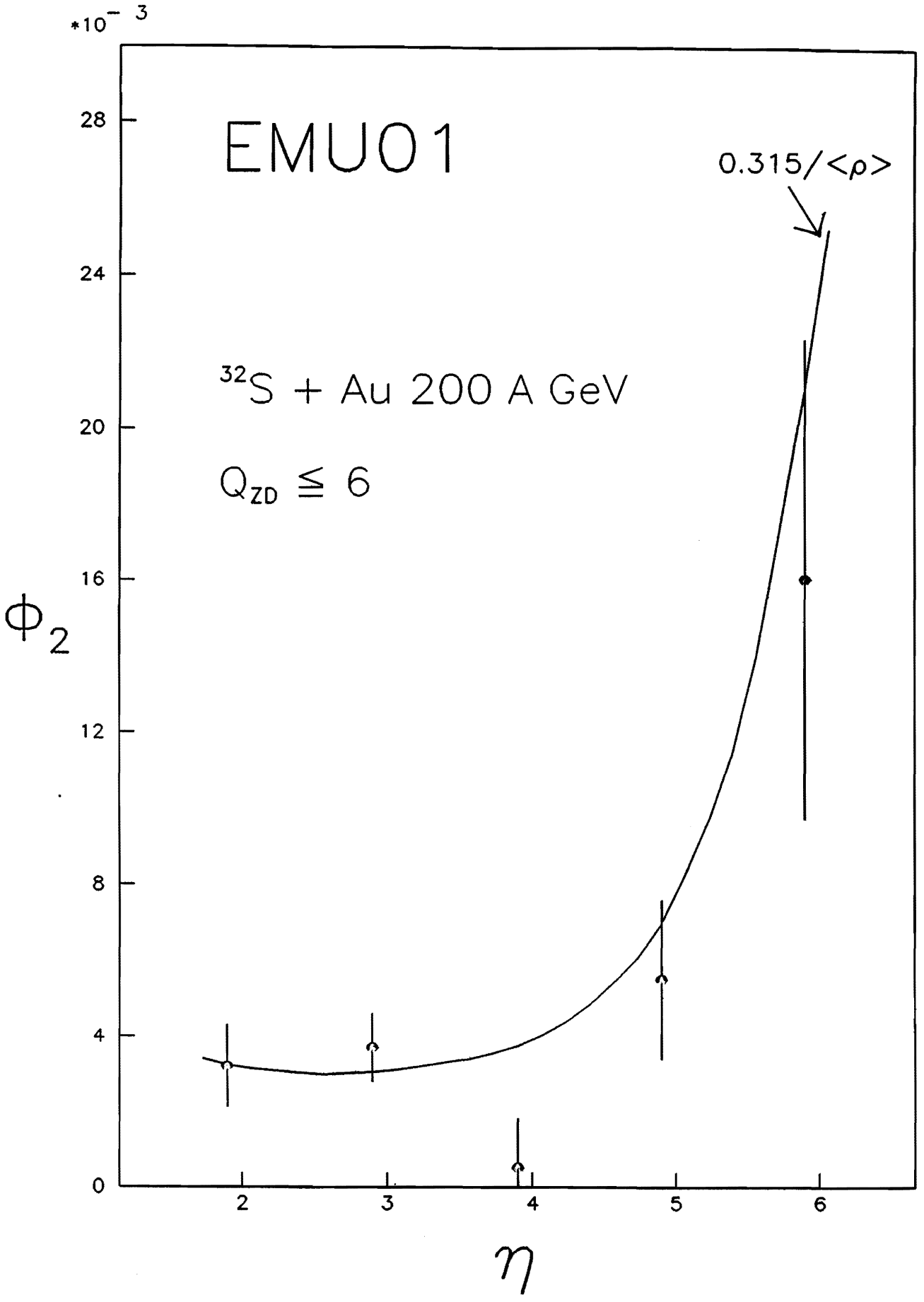
*10⁻ 3
28
24
20
16
12
8
4
0
EMU01
0.315/<ρ>
32S + Au 200 A GeV
QZD ≦ 6
Φ2
2
3
4
5
6
η

Fig. 7

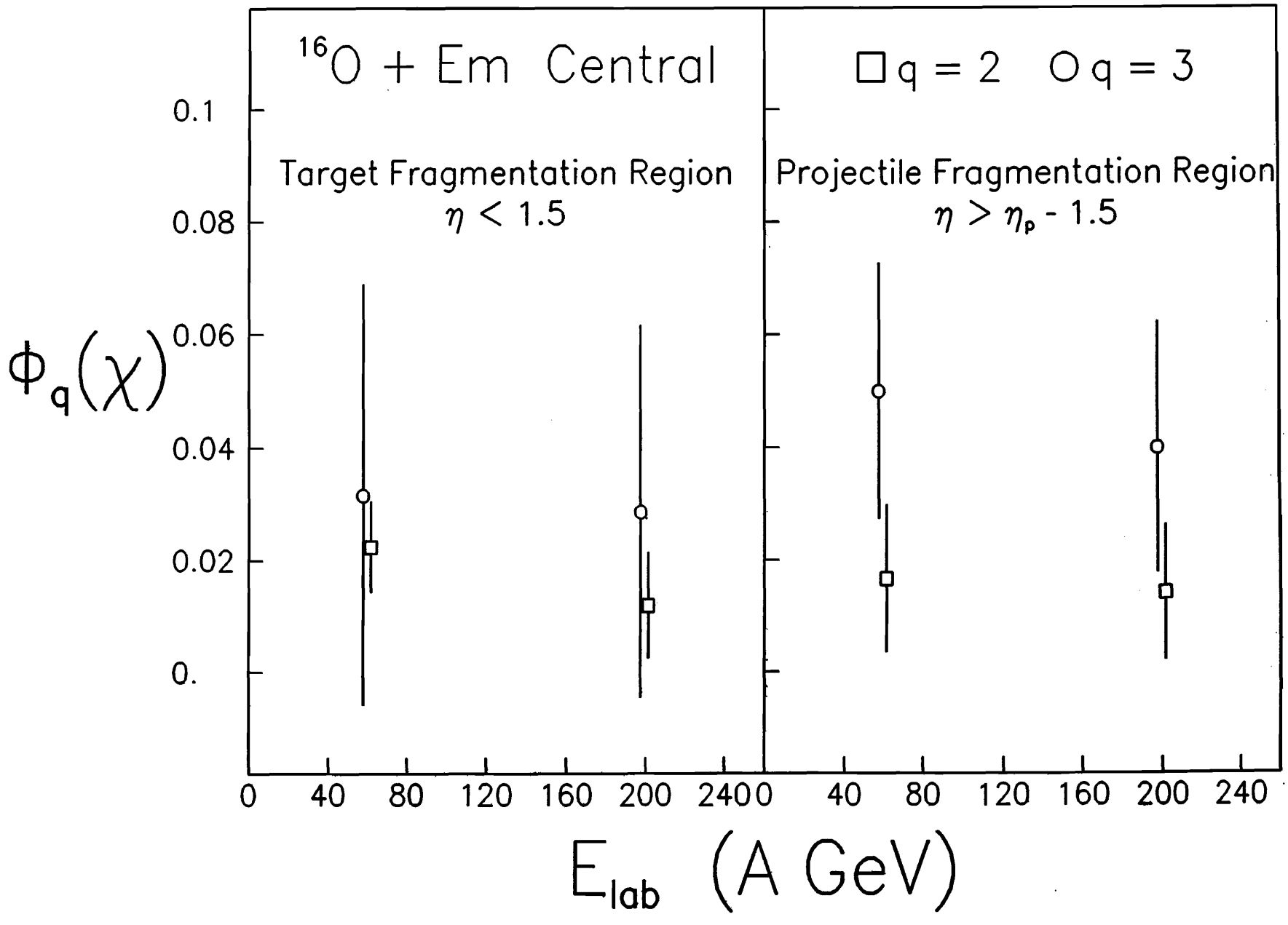
^{16}O + Em Central
□ q = 2 ○ q = 3
Target Fragmentation Region
$\eta < 1.5$
Projectile Fragmentation Region
$\eta > \eta_p - 1.5$
$\Phi_q(\chi)$
0.1
0.08
0.06
0.04
0.02
0.
0
40
80
120
160
200
240
E_{lab} (A GeV)

Fig. 8

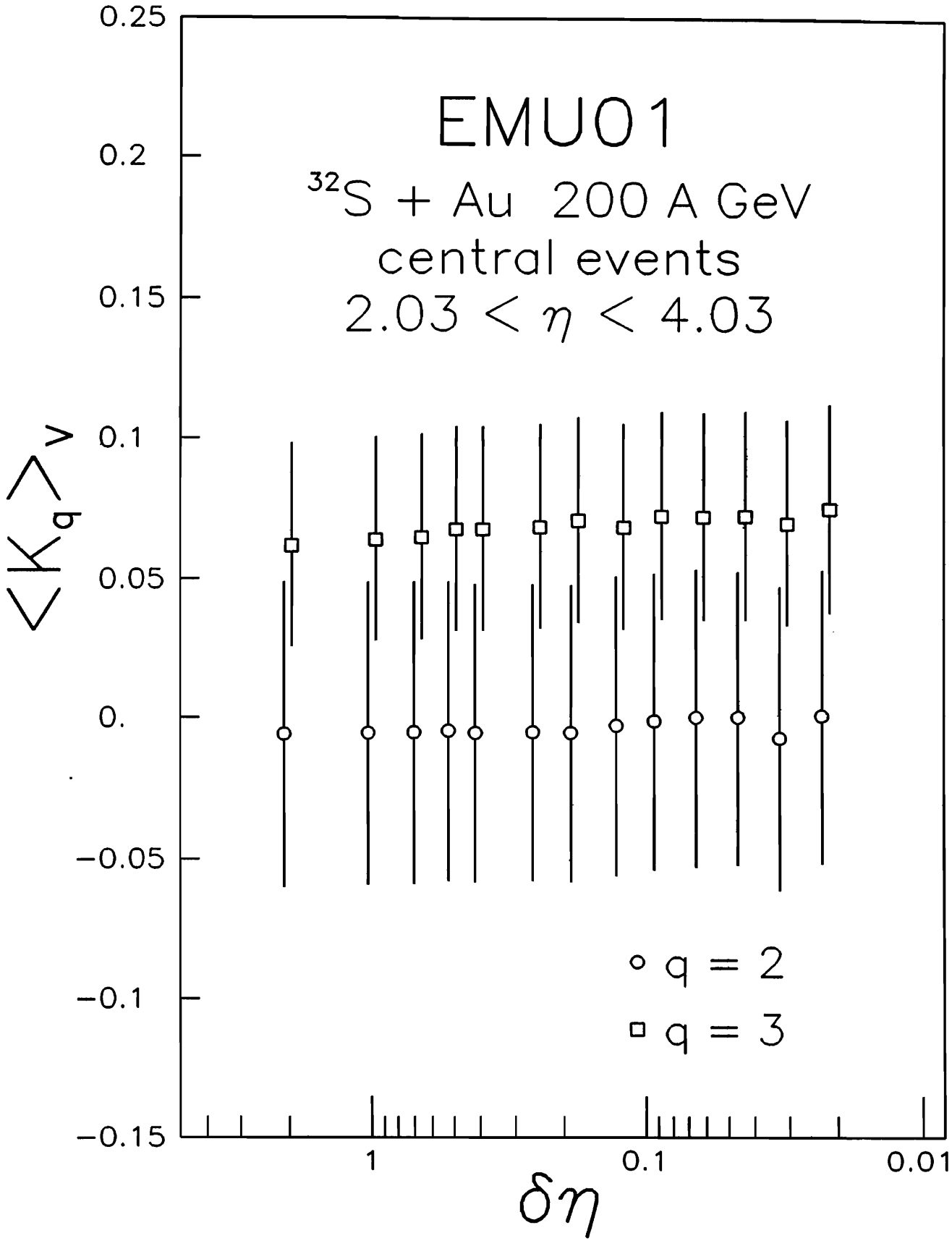
EMU01
^{32}S + Au 200 A GeV
central events
$2.03 < \eta < 4.03$
$\langle K_q \rangle_v$
0.25
0.2
0.15
0.1
0.05
0.
−0.05
−0.1
−0.15
1
0.1
0.01
$\delta\eta$
q = 2
q = 3

Fig. 9

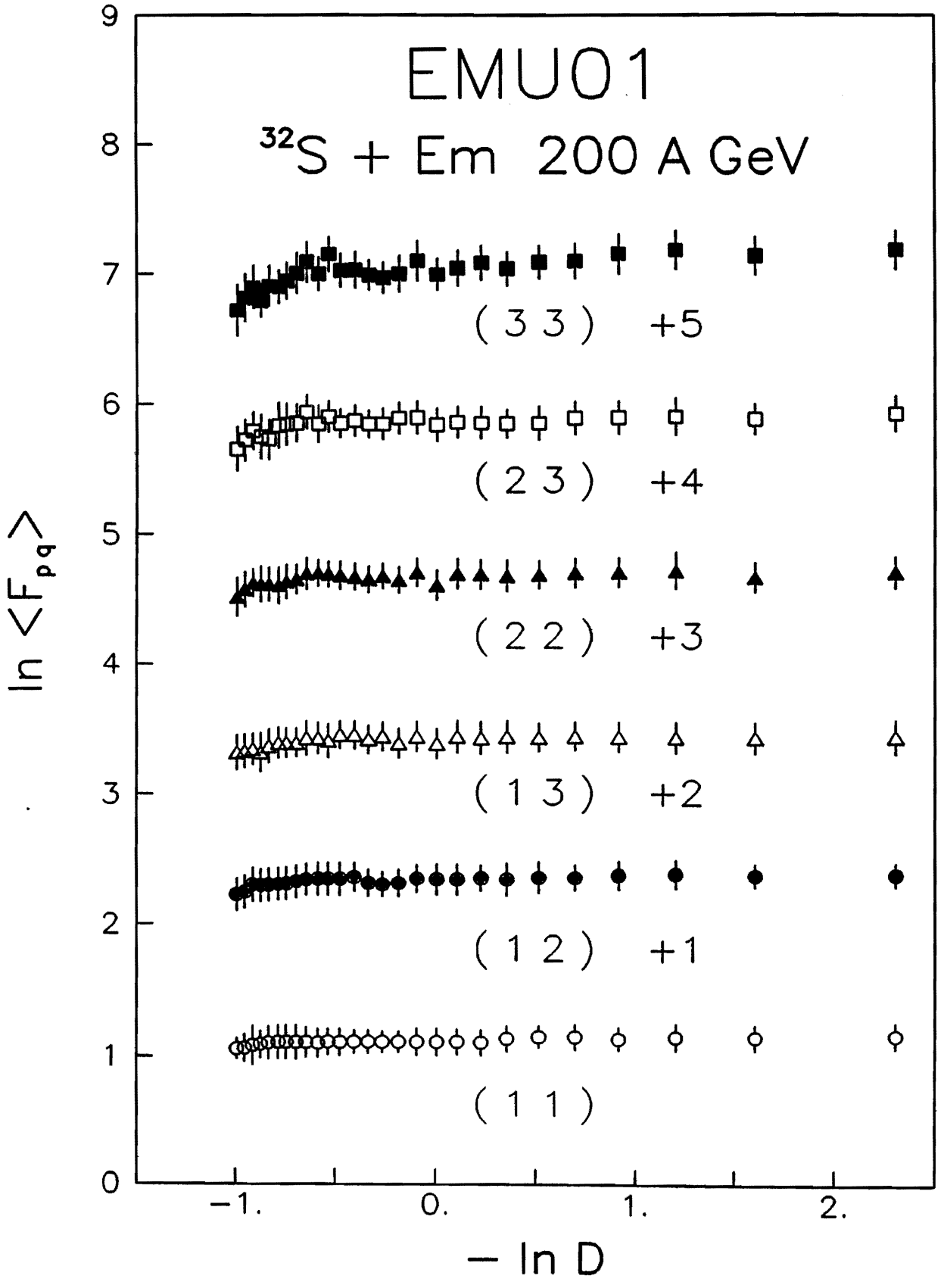
EMU01
32S + Em 200 A GeV
(3 3) +5
(2 3) +4
(2 2) +3
(1 3) +2
(1 2) +1
(1 1)
ln <Fpq>
− ln D
0
1
2
3
4
5
6
7
8
9
−1.
0.
1.
2.

Fig. 10

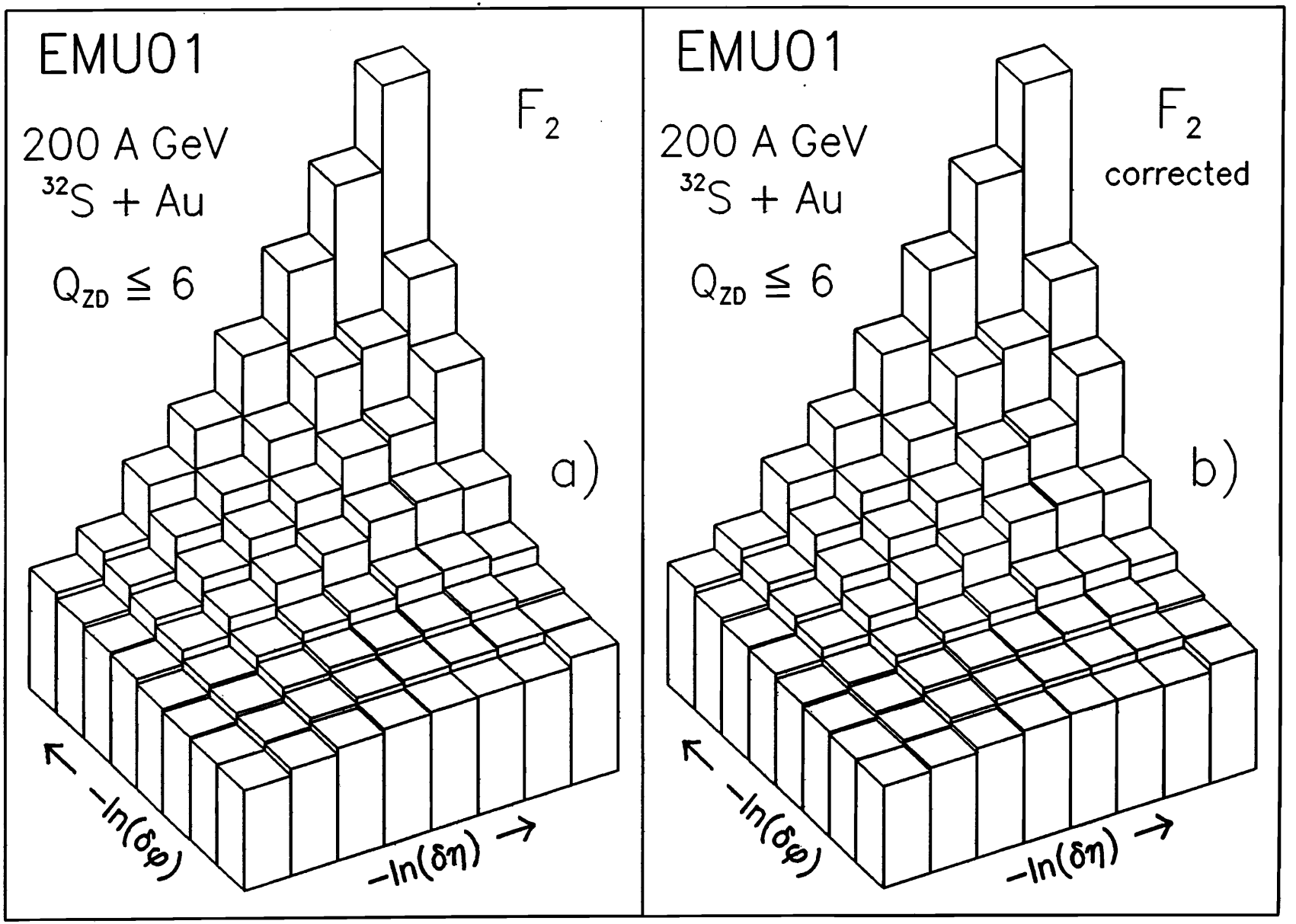
EMU01
200 A GeV
32S + Au
QZD ≤ 6
F2
a)
-ln(δφ)
-ln(δη)
EMU01
200 A GeV
32S + Au
QZD ≤ 6
F2
corrected
b)
-ln(δφ)
-ln(δη)

Fig. 11

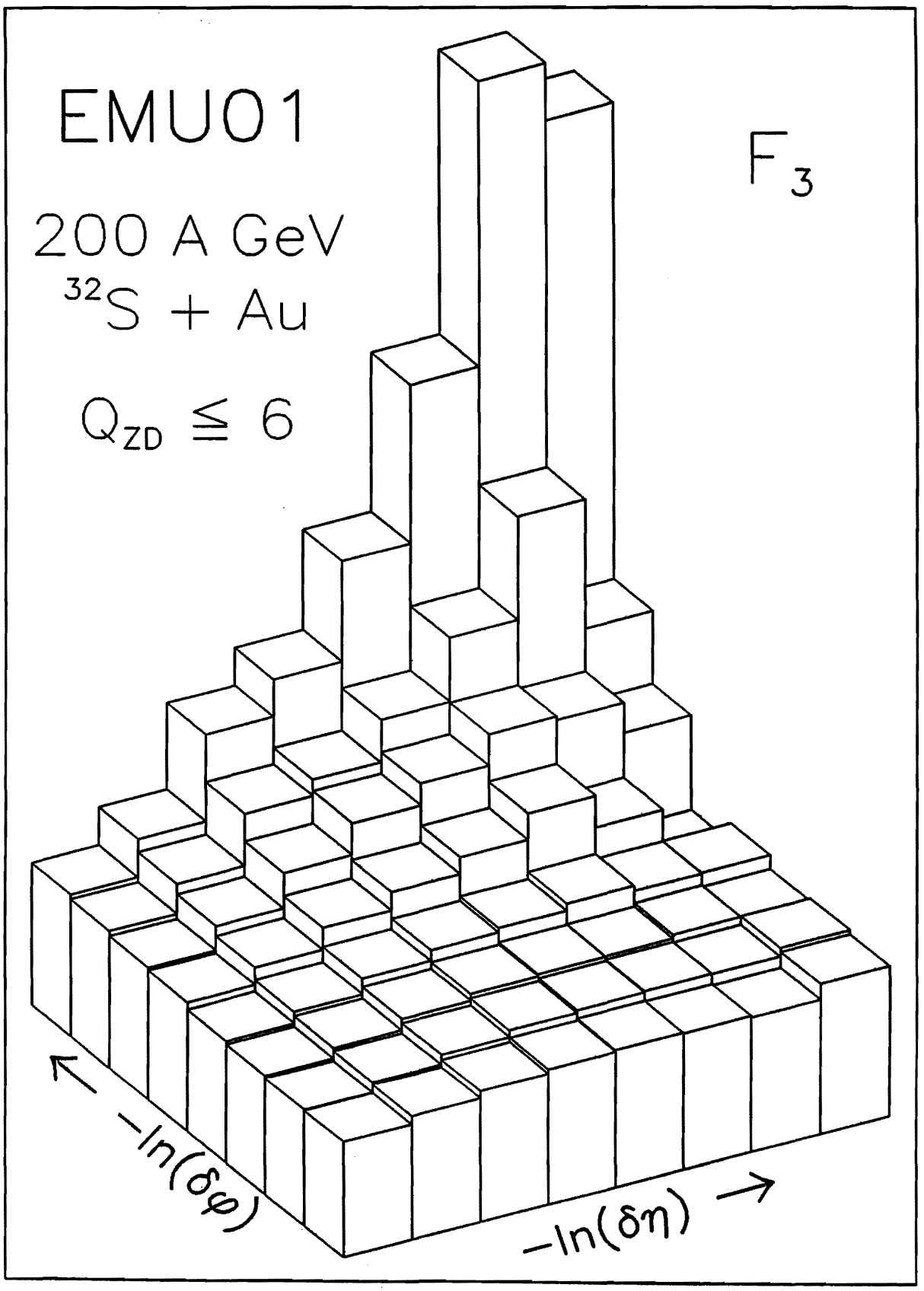

Fig. 12

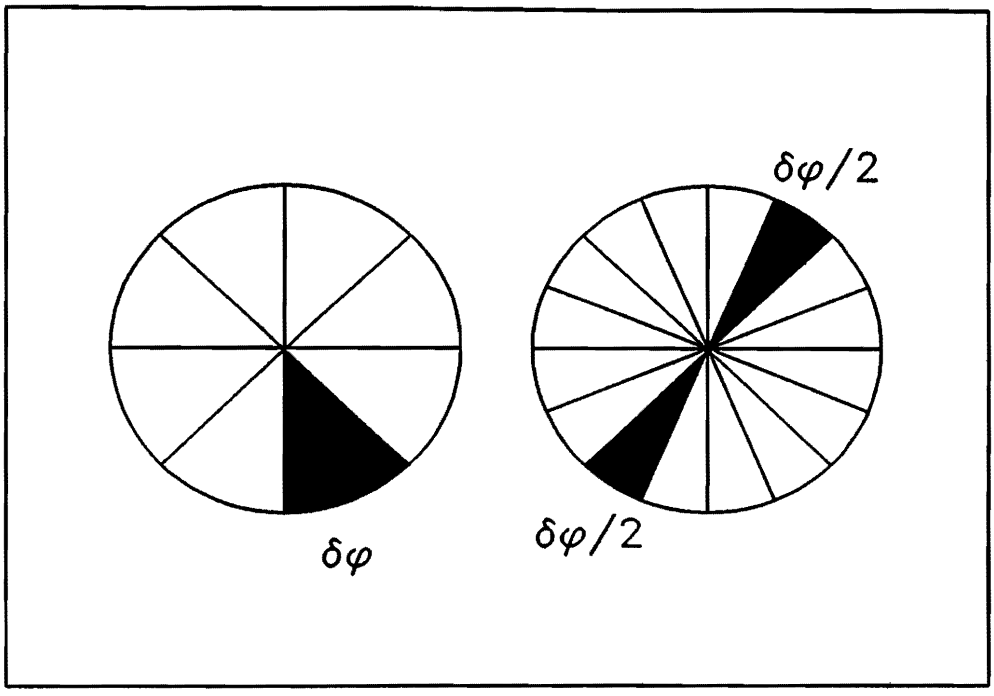

Fig. 13

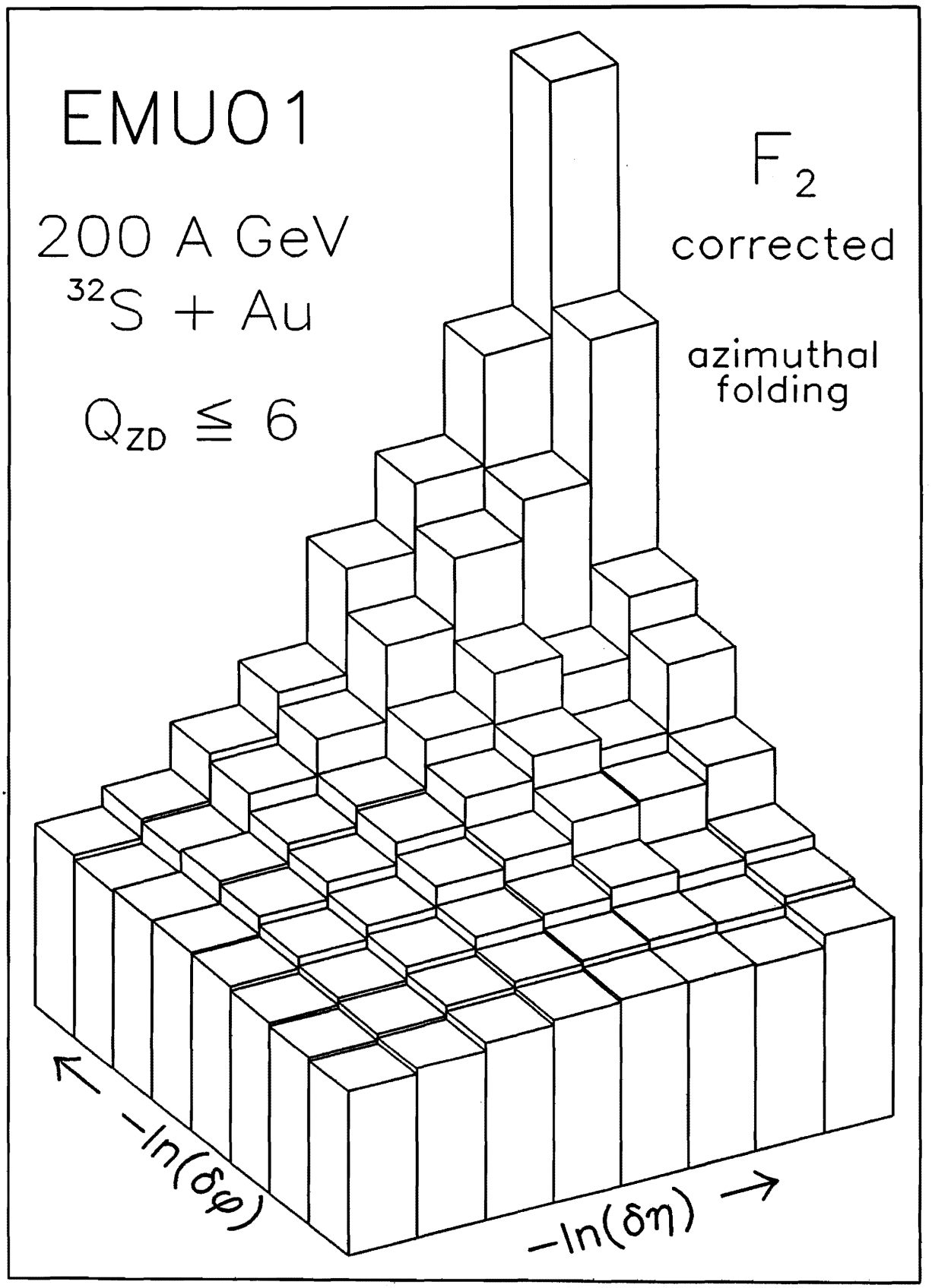
EMU01
200 A GeV
^{32}S + Au
$Q_{ZD} \leq 6$
F_2
corrected
azimuthal
folding
$-\ln(\delta\varphi)$
$-\ln(\delta\eta)$

Fig. 14

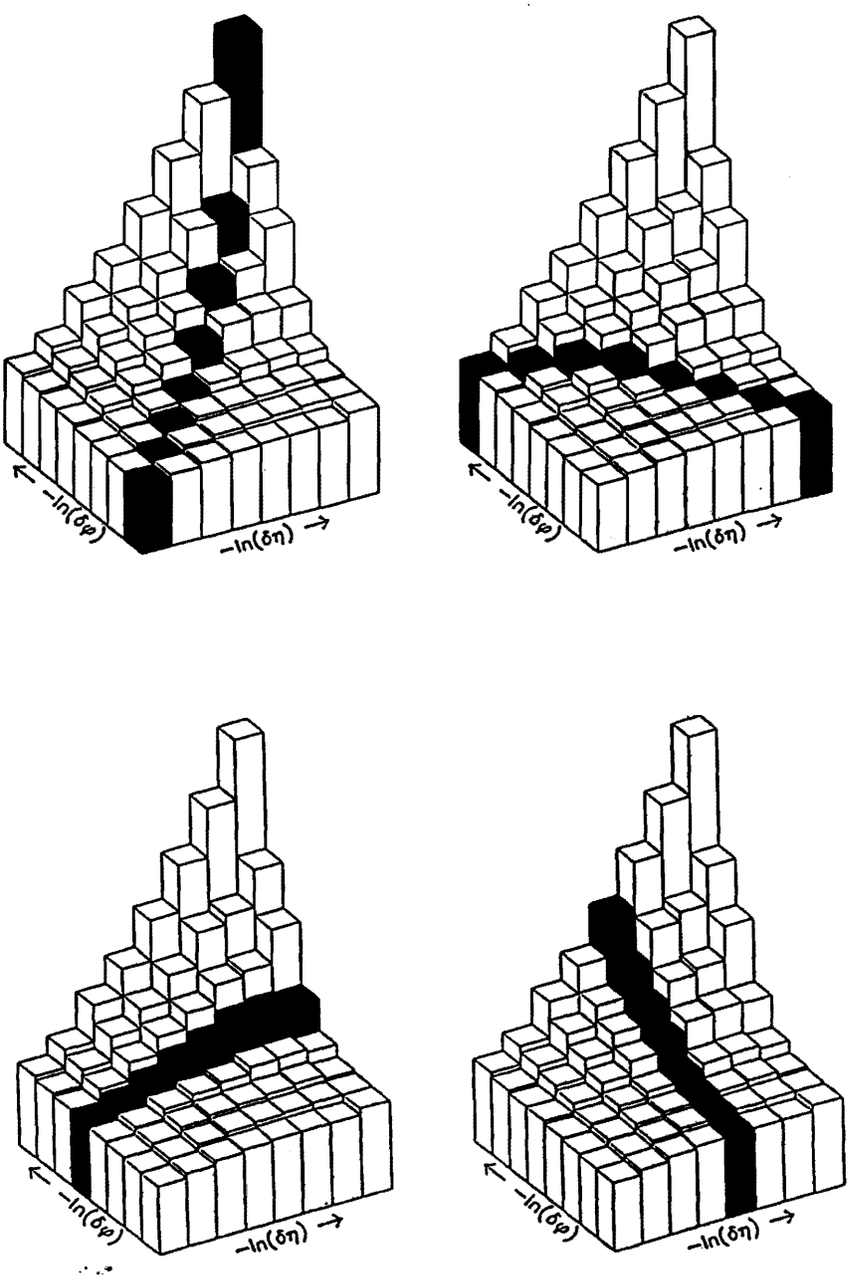
$-\ln(\delta\varphi)$
$-\ln(\delta\eta)$
$-\ln(\delta\varphi)$
$-\ln(\delta\eta)$
$-\ln(\delta\varphi)$
$-\ln(\delta\eta)$
$-\ln(\delta\varphi)$
$-\ln(\delta\eta)$

Fig. 15

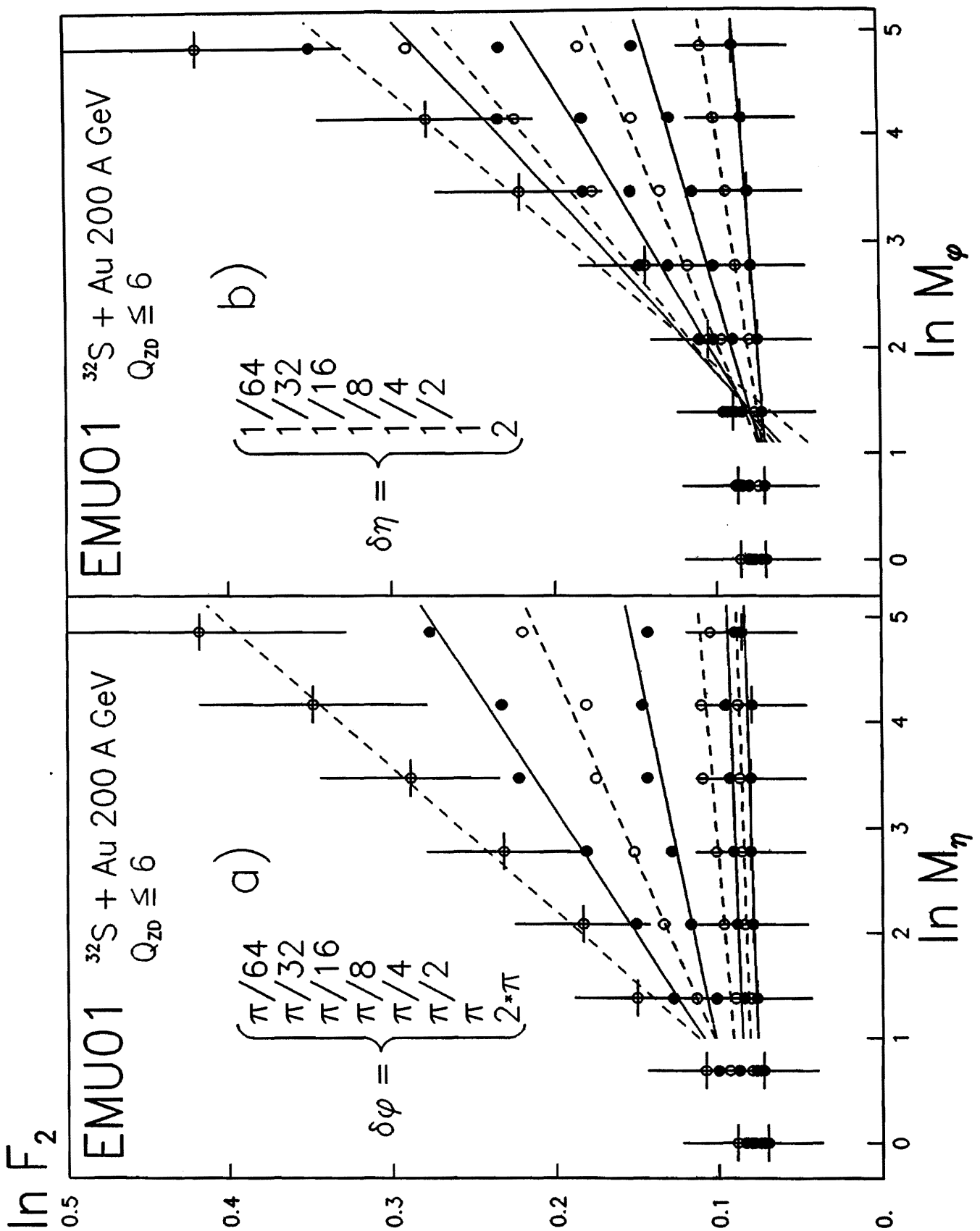
ln F2
EMU01 32S + Au 200 A GeV
QZD ≤ 6
a)
δφ = π/64 π/32 π/16 π/8 π/4 π/2 π 2*π
ln Mη
b)
δη = 1/64 1/32 1/16 1/8 1/4 1/2 1 2
ln Mφ

Fig. 16

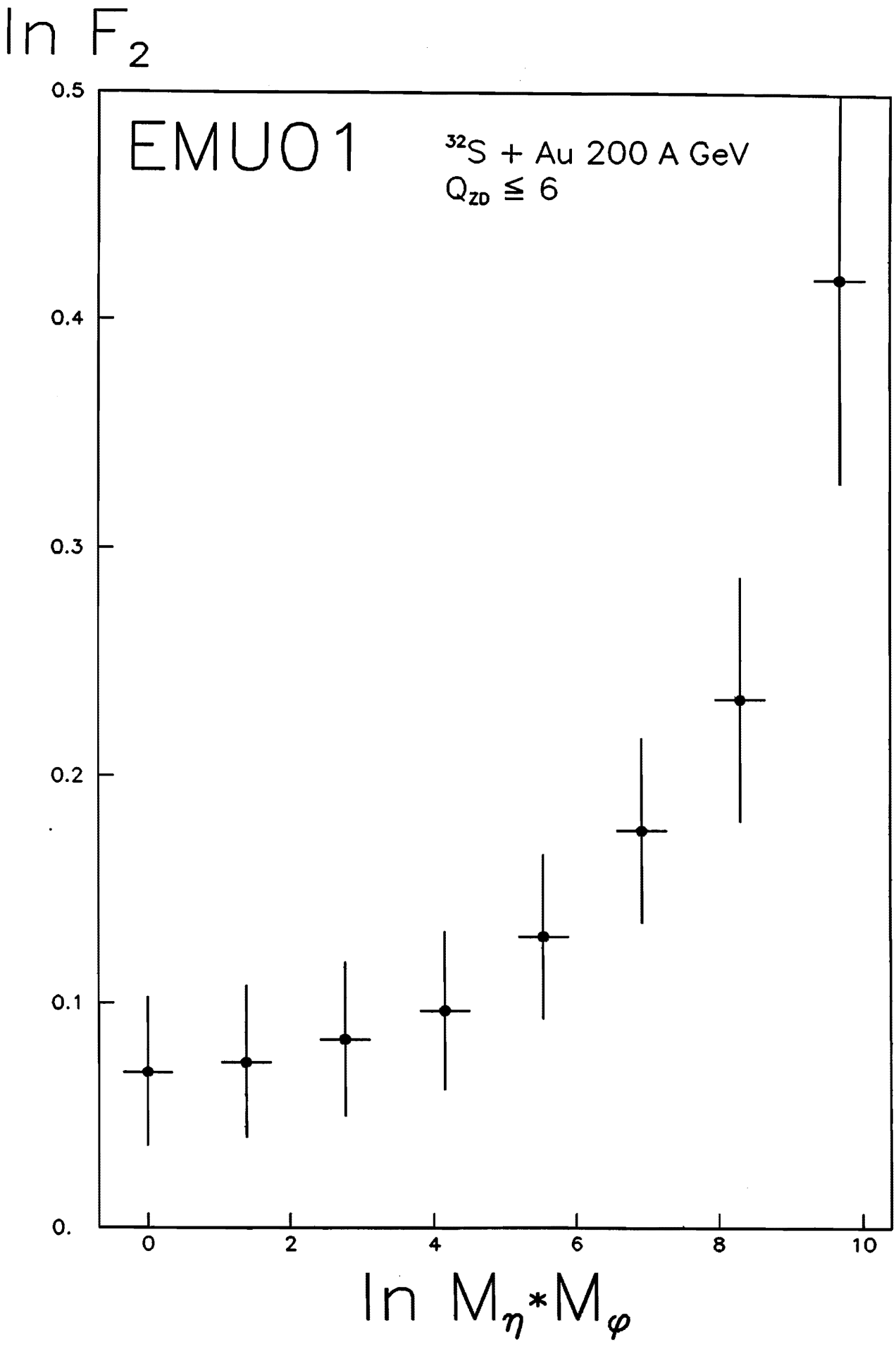
ln F_2
EMU01
^{32}S + Au 200 A GeV
$Q_{ZD} \leq 6$
0.5
0.4
0.3
0.2
0.1
0.
0
2
4
6
8
10
ln $M_\eta * M_\varphi$

Fig. 17

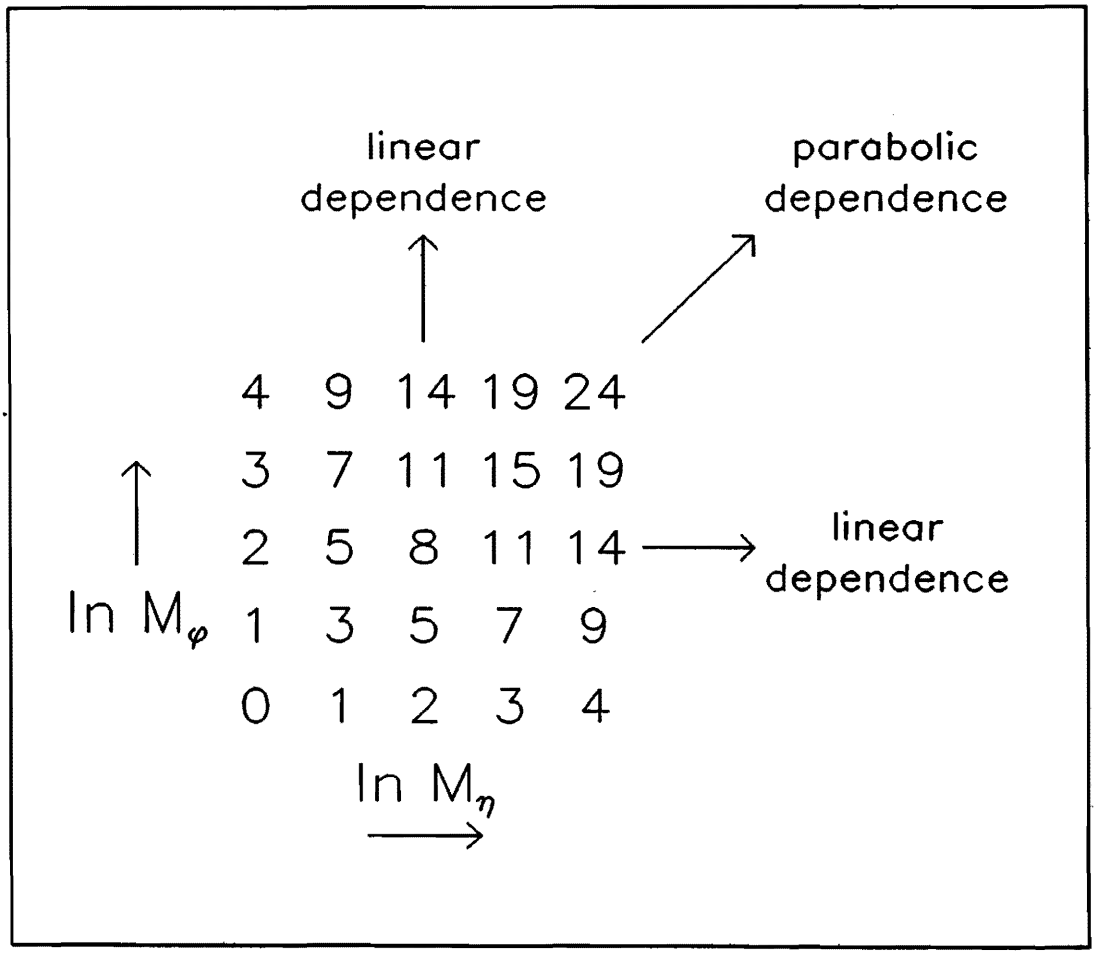
linear
dependence
parabolic
dependence
4 9 14 19 24
3 7 11 15 19
2 5 8 11 14
linear
dependence
ln M_φ
1 3 5 7 9
0 1 2 3 4
ln M_η

Fig. 18

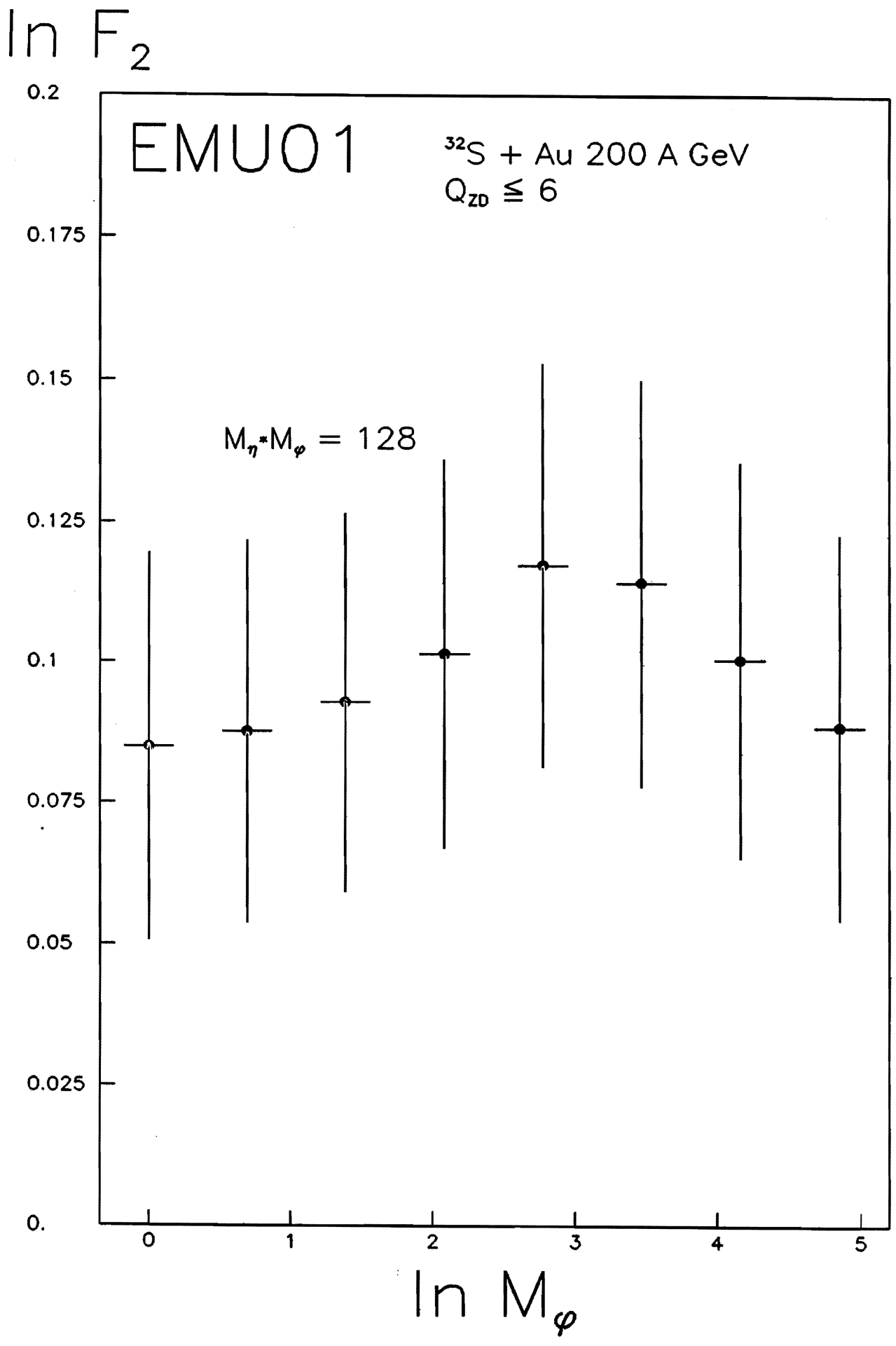
ln F_2
EMU01
^{32}S + Au 200 A GeV
$Q_{ZD} \leq 6$
$M_\eta * M_\varphi = 128$
0.2
0.175
0.15
0.125
0.1
0.075
0.05
0.025
0.
0
1
2
3
4
5
ln M_φ

Fig. 19

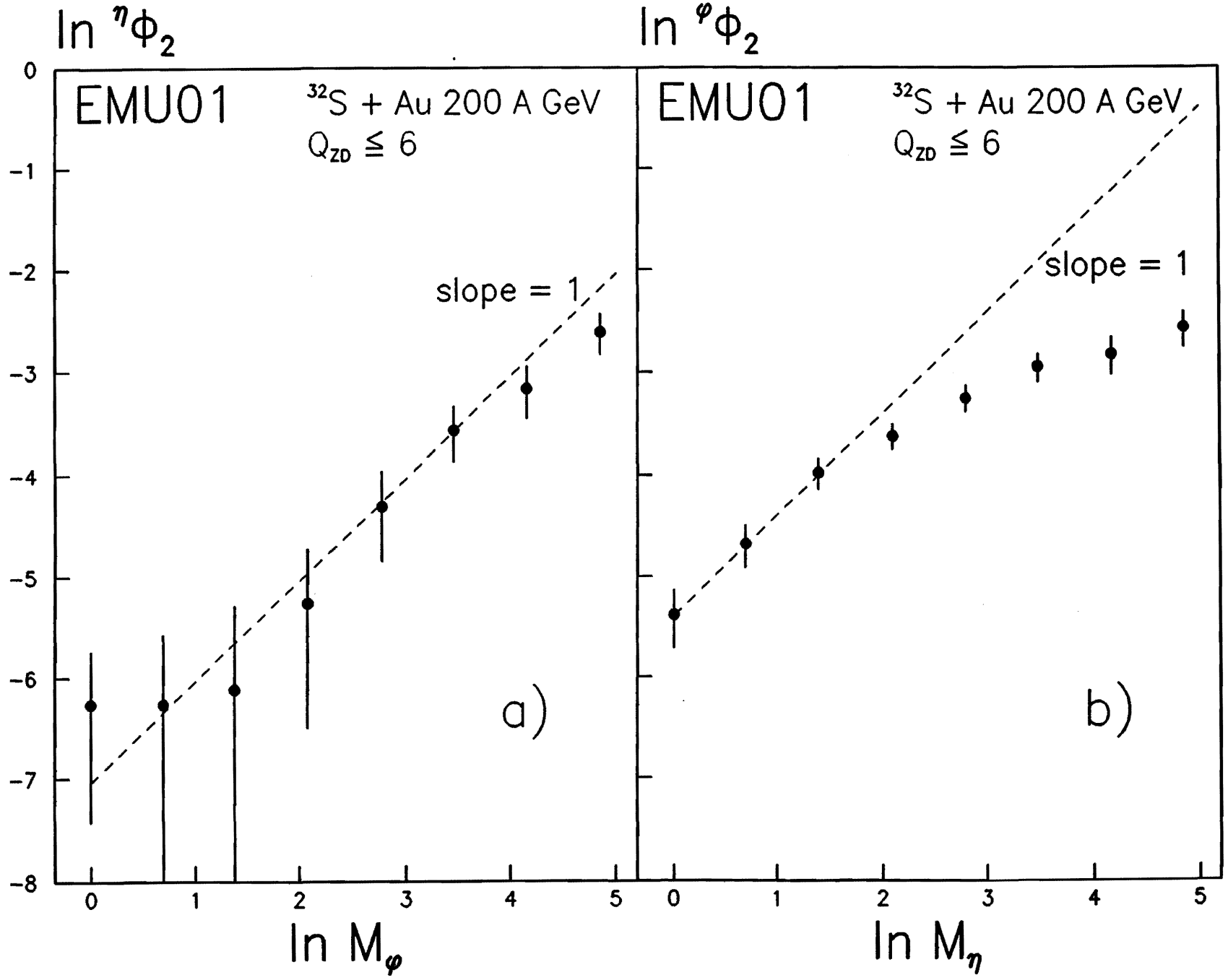
ln $^{\eta}\Phi_2$
EMU01
^{32}S + Au 200 A GeV
$Q_{ZD} \leq 6$
slope = 1
a)
ln M_{φ}
ln $^{\varphi}\Phi_2$
EMU01
^{32}S + Au 200 A GeV
$Q_{ZD} \leq 6$
slope = 1
b)
ln M_{η}

Fig. 20

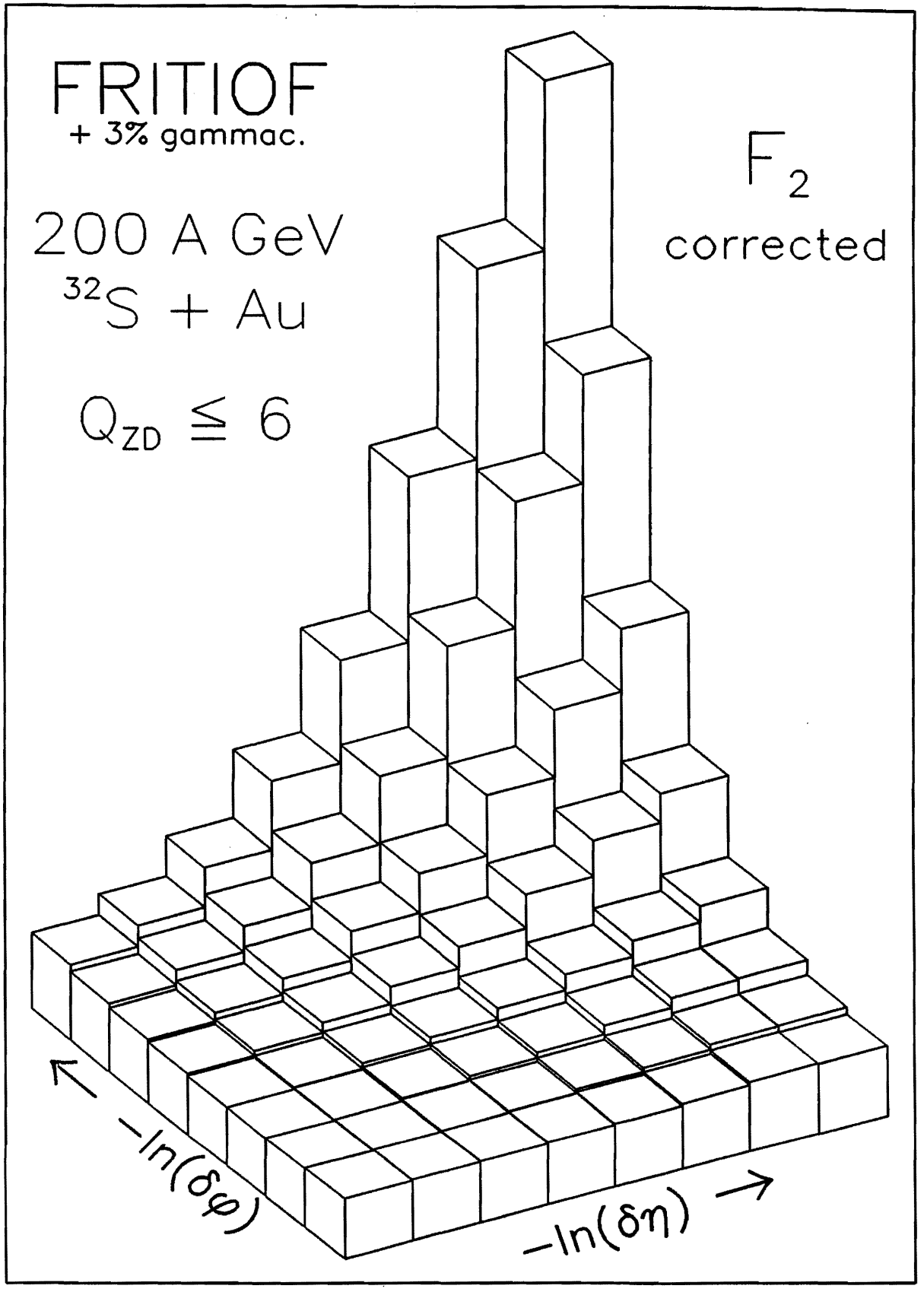

Fig. 21

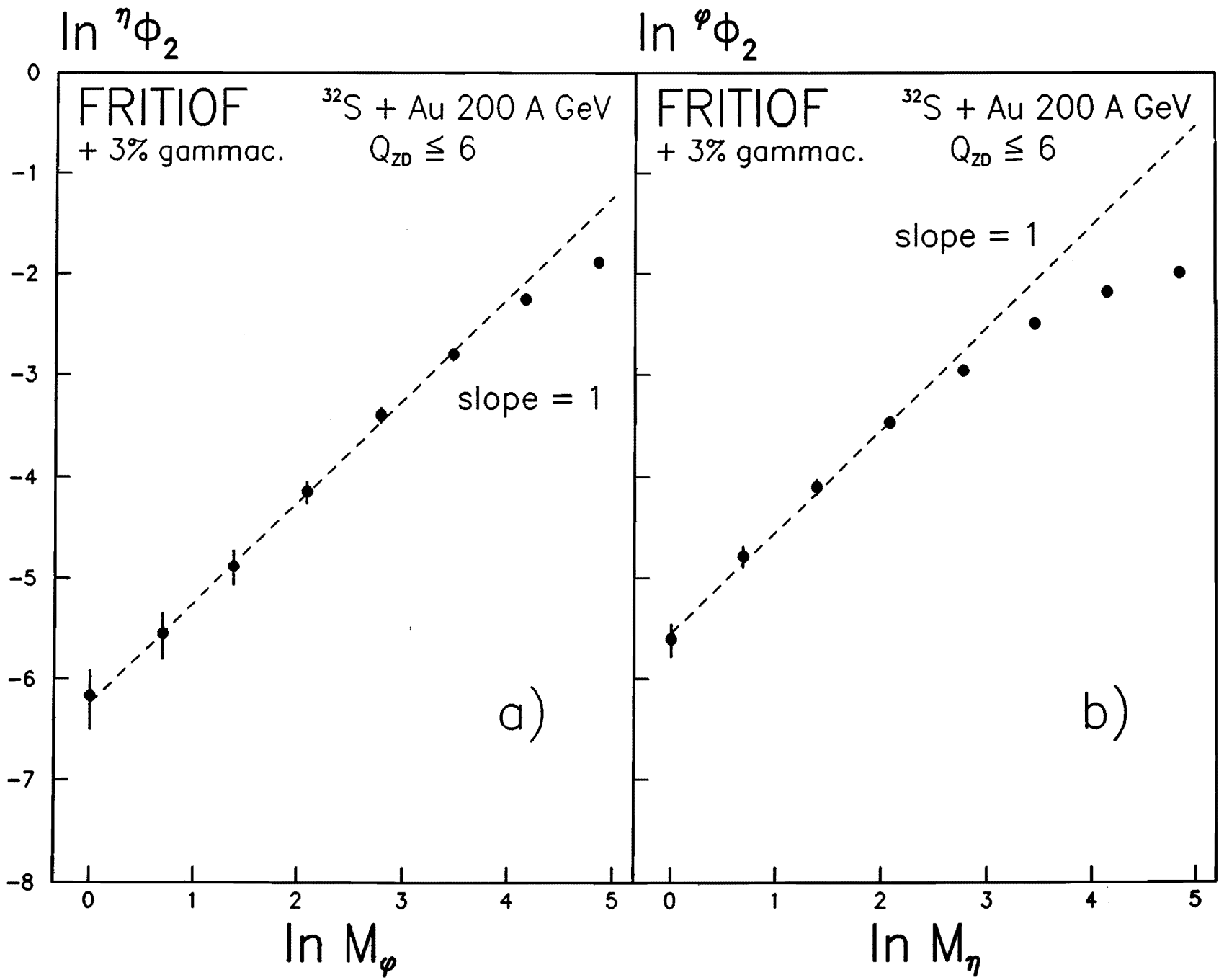
ln $^{\eta}\Phi_2$
FRITIOF
+ 3% gammac.
^{32}S + Au 200 A GeV
$Q_{ZD} \leqq 6$
slope = 1
a)
ln M_{φ}
ln $^{\varphi}\Phi_2$
FRITIOF
+ 3% gammac.
^{32}S + Au 200 A GeV
$Q_{ZD} \leqq 6$
slope = 1
b)
ln M_{η}
0
-1
-2
-3
-4
-5
-6
-7
-8
0
1
2
3
4
5

Fig. 22

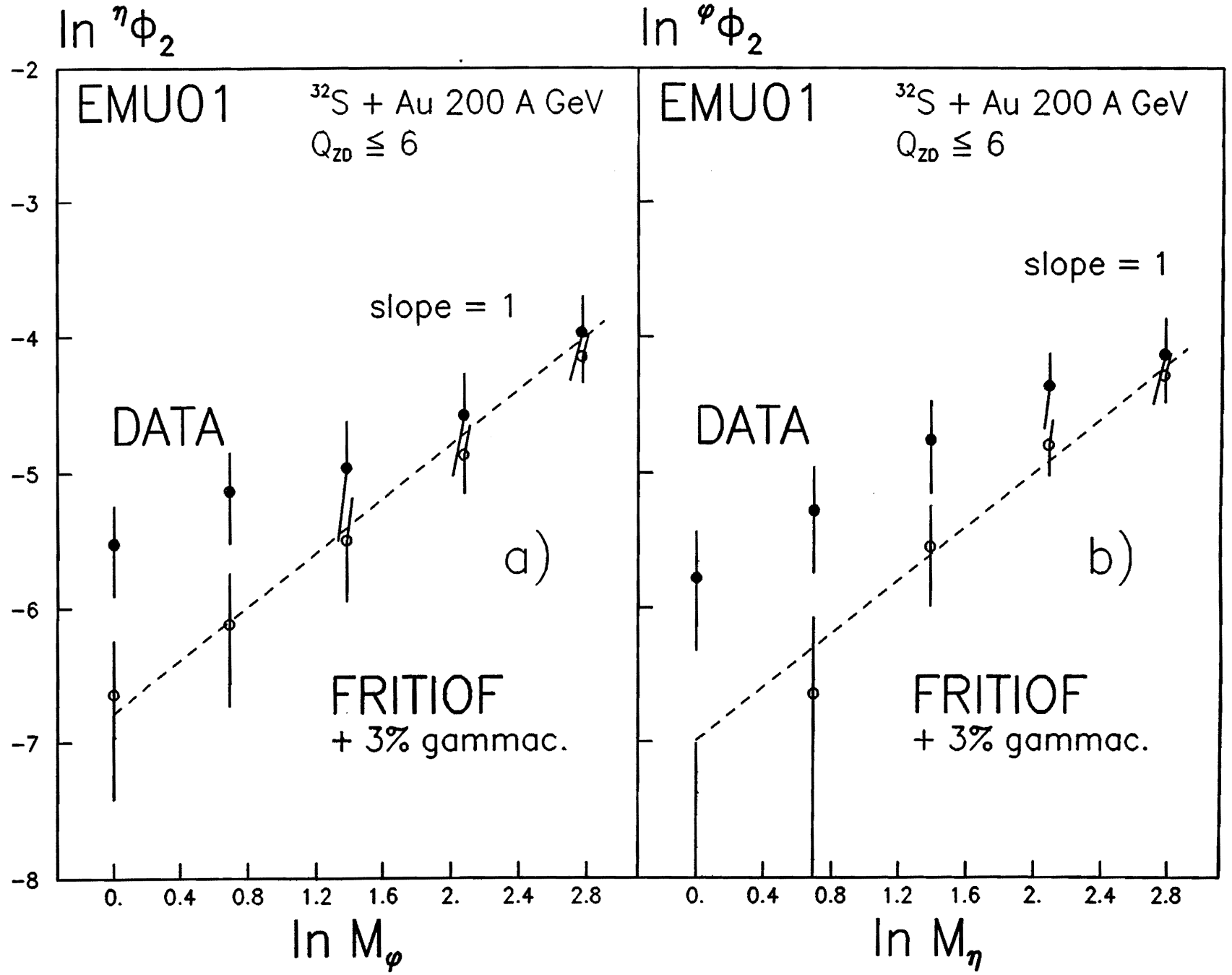
ln $^{\eta}\Phi_2$
ln $^{\varphi}\Phi_2$
EMU01
^{32}S + Au 200 A GeV
$Q_{ZD} \leq 6$
slope = 1
DATA
a)
b)
FRITIOF
+ 3% gammac.
-2
-3
-4
-5
-6
-7
-8
0.
0.4
0.8
1.2
1.6
2.
2.4
2.8
ln M_{φ}
ln M_{η}

Fig. 23

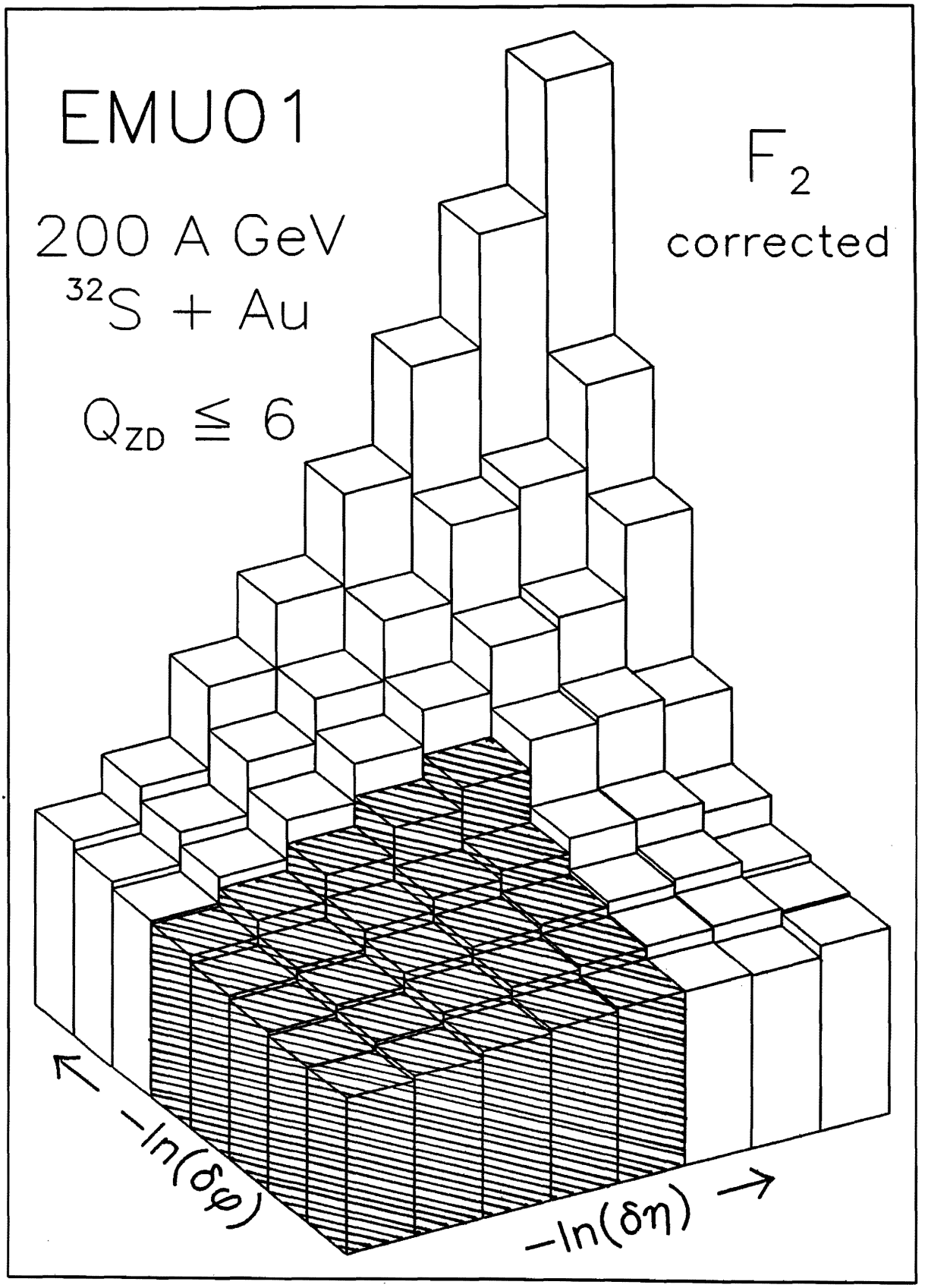
EMU01
200 A GeV
^{32}S + Au
$Q_{ZD} \leq 6$
F_2
corrected
$-\ln(\delta\varphi)$
$-\ln(\delta\eta)$

Fig. 24

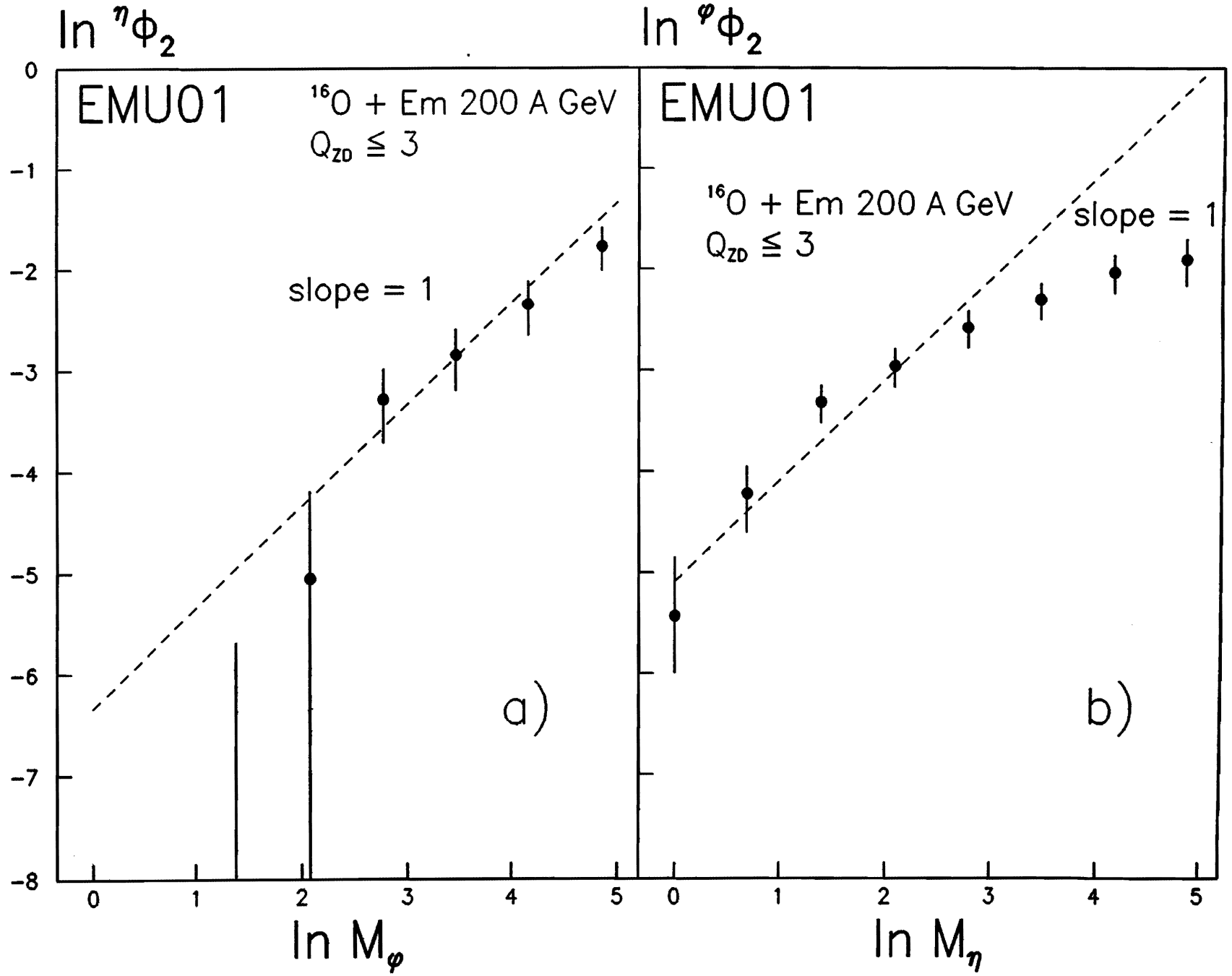
ln $^{\eta}\Phi_2$
EMU01
^{16}O + Em 200 A GeV
$Q_{ZD} \leq 3$
slope = 1
a)
ln M_{φ}
ln $^{\varphi}\Phi_2$
EMU01
^{16}O + Em 200 A GeV
$Q_{ZD} \leq 3$
slope = 1
b)
ln M_{η}

Fig. 25

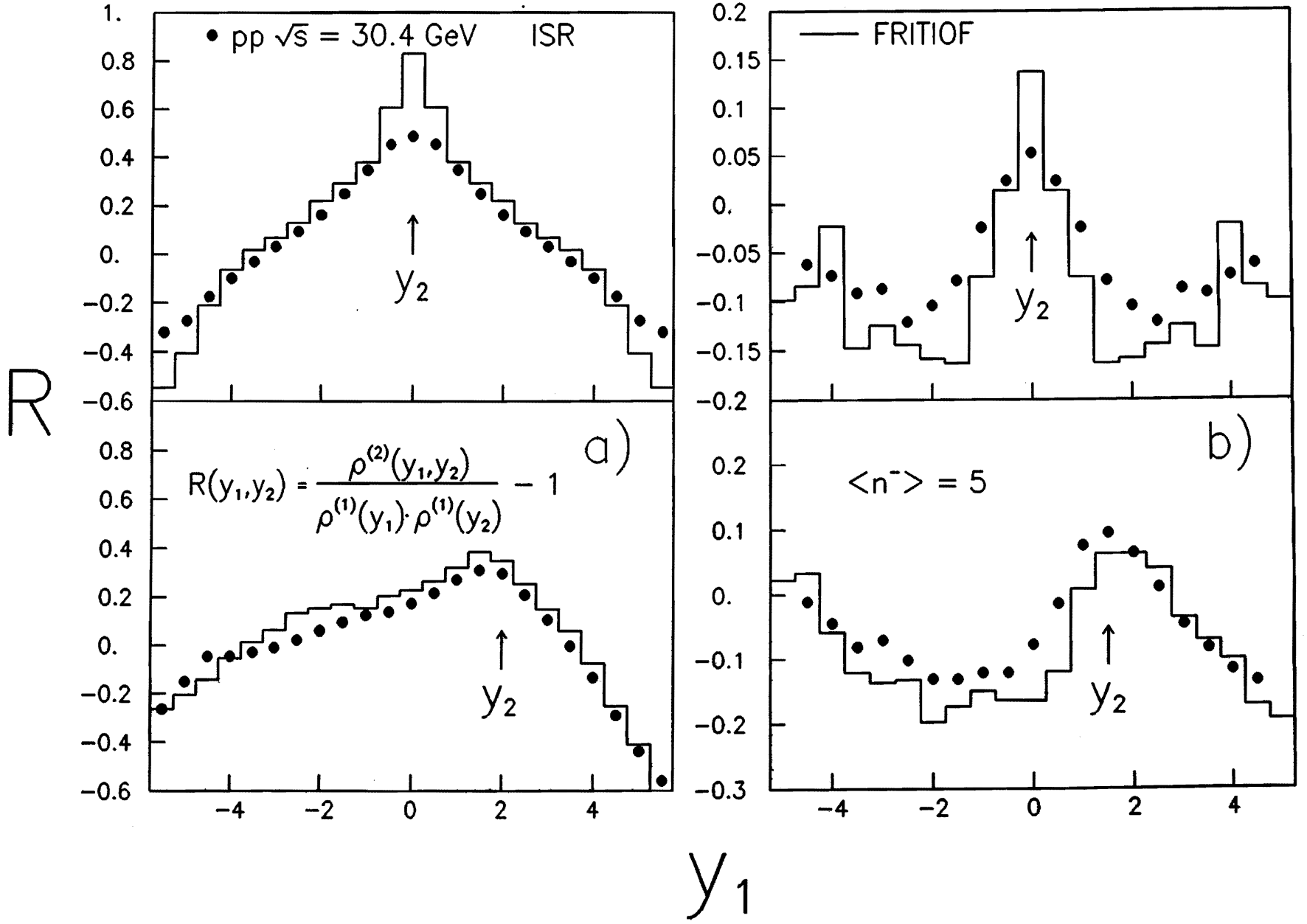
• pp √s = 30.4 GeV ISR
— FRITIOF
a)
b)
$R(y_1,y_2) = \frac{\rho^{(2)}(y_1,y_2)}{\rho^{(1)}(y_1)\cdot\rho^{(1)}(y_2)} - 1$
<n⁻> = 5
y2
R
y1

Fig. 26

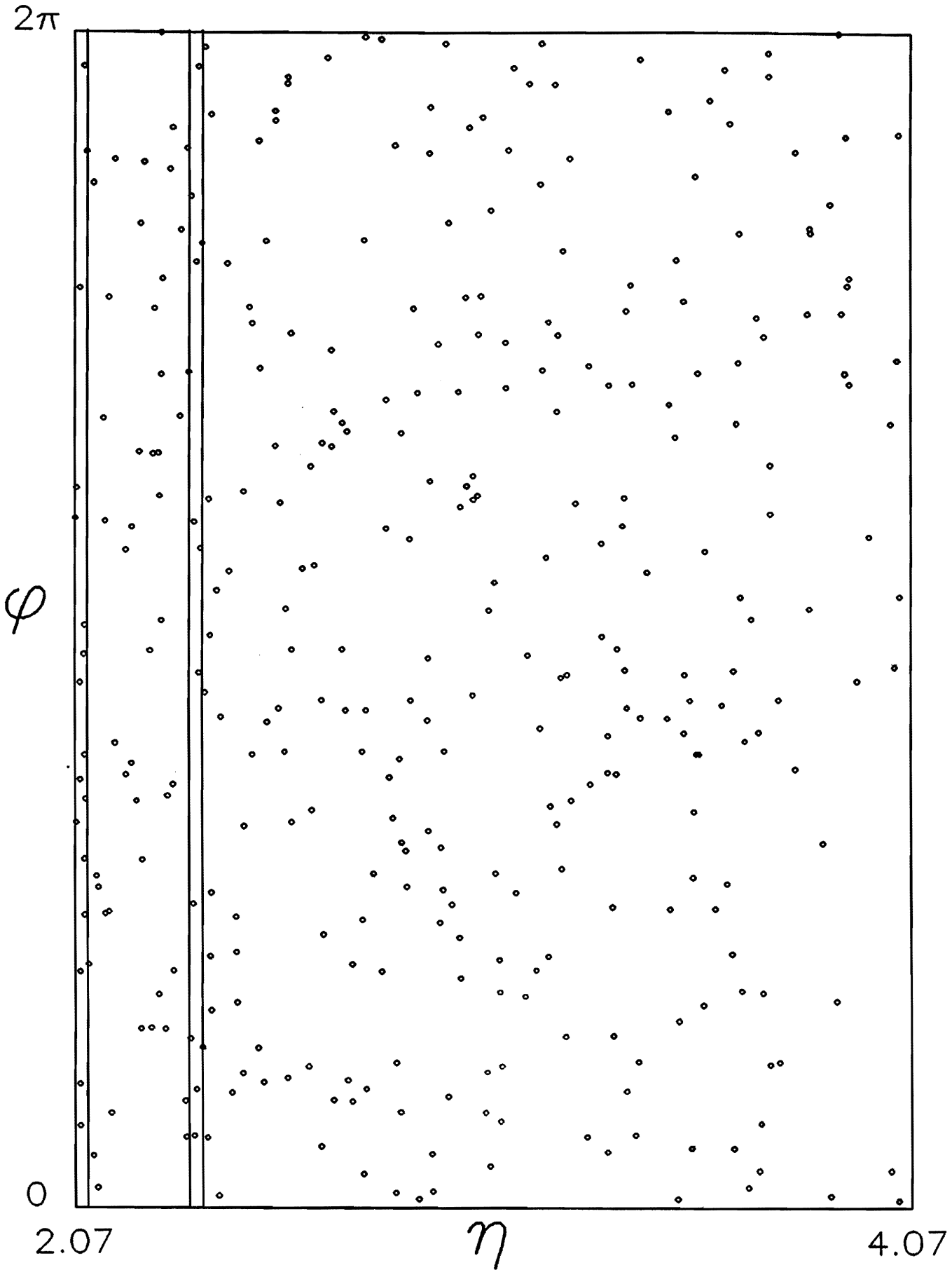

Fig. 27

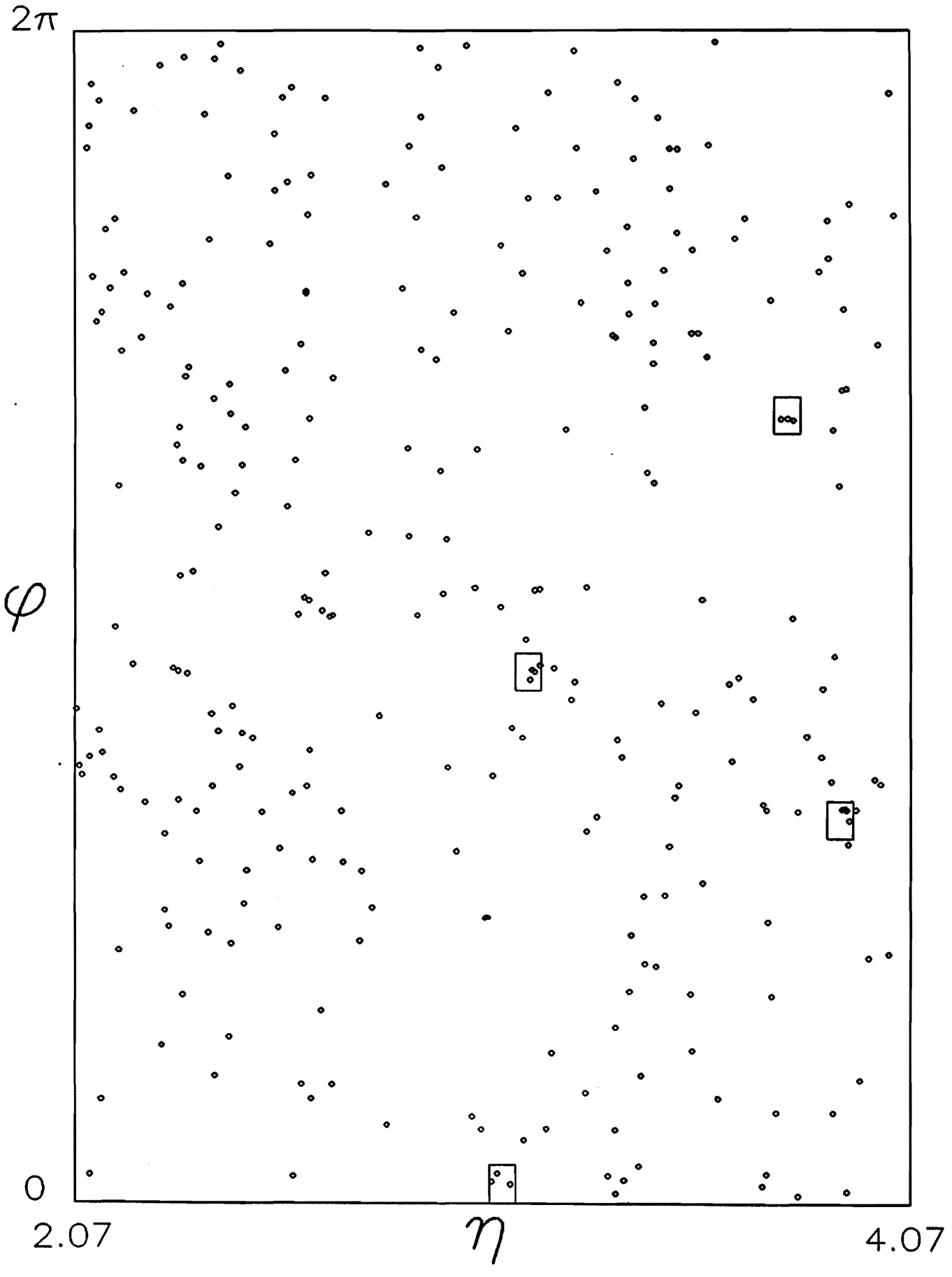

Fig. 28